NASA
Technical
Paper
2612

October 1986

Effects of Thermal Cycling on Graphite-Fiber-Reinforced 6061 Aluminum

Gregory A. Dries and
Stephen S. Tompkins

NASA

Effects of Thermal Cycling on Graphite-Fiber-Reinforced 6061 Aluminum

Gregory A. Dries
PRC Kentron, Inc.
Hampton, Virginia

Stephen S. Tompkins
Langley Research Center
Hampton, Virginia

Summary

Graphite-reinforced aluminum alloy (Gr/Al) metal-matrix composites are leading candidates for structural components in high precision space structures. This application requires materials with low values of thermal expansion and high specific stiffnesses, which must remain stable during exposures to the space environment for periods extending to 20 years. The effects of thermal cycling on the thermal expansion behavior and mechanical properties of Gr/6061 Al composites, as fabricated and after thermal processing to eliminate thermal strain hysteresis, have been investigated. Two groups of composites were studied; one group was fabricated by hot roll bonding and the other by diffusion bonding. Processing significantly reduced the strain hysteresis during thermal cycling in both groups of composites and improved the ultimate tensile strength and modulus in the diffusion-bonded material. Thermal cycling stabilized the as-fabricated composites by reducing the residual fabrication stress and also increased the matrix strength by metallurgical aging. The thermal expansion behavior of both groups of composites after processing was insensitive to thermal cycling. Data scatter was too large to determine effects of thermal cycling on the mechanical properties. The primary effects of processing and thermal cycling can be attributed to changes in the metallurgical condition and stress state of the matrix.

Introduction

Graphite-fiber-reinforced aluminum alloy metal-matrix composites are among the material systems being considered for structural components in dimensionally stable space structures, such as large antennas. This application requires materials with low values of thermal expansion and high specific stiffnesses, which must remain stable during exposures to the space environment for periods extending to 20 years (ref. 1). The temperature range over which a composite must be dimensionally stable in Earth orbit can be as wide as $-250°F$ to $250°F$, depending upon the thermal control systems used. Initial thermal expansion testing of graphite fiber/aluminum alloy (Gr/Al) materials over this temperature range revealed significant thermal strain hysteresis and residual dimensional changes (ref. 2). Subsequent studies (ref. 3) demonstrated that postfabrication processing can eliminate the residual dimensional changes and significantly reduce thermal strain hysteresis, thereby providing a more stable expansion behavior. Since the use of composites in dimensionally critical space structures also requires that thermal expansion properties remain constant throughout the lifetime of

the structure, further study was necessary to assess the long-term stability of thermal expansion and mechanical properties.

This report presents the results of a study of the effects of thermal cycling on properties of Gr/Al composites, both as fabricated and after processing to stabilize the thermal expansion behavior. The objectives of the study were to determine if critical composite properties would change with thermal cycling and to provide insight into the mechanisms responsible for any observed changes. The coefficient of thermal expansion, the ultimate tensile strength, the microhardness, and the elastic properties of 6061 aluminum composites reinforced with continuous Thornel P100 graphite fibers were measured as a function of thermal cycles between $-250°F$ and $250°F$ for up to 500 cycles. Changes in the properties of the as-fabricated and processed composites with thermal cycling, as related to the metallurgical temper of the aluminum matrix are discussed.

Materials and Procedures

Materials and Specimens

Single-ply, unidirectionally reinforced Gr/Al panels, fabricated by two methods, were studied. These composite panels consisted of a matrix of 6061 aluminum alloy reinforced with continuous Thornel P100 graphite fibers bonded between two 6061 aluminum foils. One set of panels was fabricated by DWA Composite Specialities, Inc., using a diffusion bonding process. A second set was fabricated by Material Concepts, Inc. (MCI), using a hot isothermal roll bonding technique (Rapi-Press). The precursor composite tows (metal-impregnated graphite fiber bundles) used by both manufacturers in these composites were fabricated by MCI and consisted of 0.00043-in.-diameter pitch-base graphite fibers from Union Carbide Corporation impregnated with 6061 aluminum alloy. Each tow contained approximately 2000 separate fibers.

Typical optical micrographs of the cross sections of the composite laminates are shown in figure 1. Each panel had 0.0015-in.-thick surface foils of unreinforced 6061 aluminum. The diffusion-bonded panels measured 12 in. by 12 in., with a nominal thickness of 0.025 in. and a fiber volume fraction of about 0.41. The Mg and Si levels in the Al matrix after diffusion bonding were 0.35 percent by weight and 0.35 percent by weight, respectively (ref. 4). The hot-roll-bonded panels measured 3 in. by 13 in., with a nominal thickness of 0.025 in. and a fiber volume fraction of about 0.39. The Mg and Si levels in the Al matrix after roll bonding were 0.33 percent by weight and 0.39 percent by weight, respectively (ref. 4). The

)

elemental analyses of the composites were performed using atomic absorption spectroscopy.

The measured concentrations of Mg and Si in both the diffusion-bonded and hot-roll-bonded Gr/Al composites were less than those nominally specified for wrought 6061 Al. Although the reasons for the below nominal matrix chemistries are not fully understood, the segregation of solute elements back into the melt during the manufacturing of the composite tows is one theory being advanced. Another theory attributes the losses of important elements to a vaporization mechanism. Since the depleted elements are the primary constituents responsible for the strength of 6061 Al, their below nominal concentrations result in below nominal values of the mechanical properties of the matrix (ref. 4).

Tensile-test specimens were machined from the panels of each composite. Longitudinal specimens were 6.0 in. long by 0.5 in. wide and transverse specimens were 6.0 in. long by 1.0 in. wide. A schematic diagram of a typical specimen with adhesively bonded fiberglass gripping tabs is shown in figure 2(a). Gripping tabs were not used on the transverse specimens because the applied loads were much lower than on the longitudinal specimens, and therefore less gripping pressure was necessary. Thermal expansion specimens were approximately 3.0 in. long by 1.0 in. wide, with the fibers oriented longitudinally as shown in figure 2(b). The ends of each specimen were rounded and beveled to provide single-point contact in the dilatometer.

Selected specimens were processed with a heat treatment and a cryogenic stress relief treatment (as detailed in ref. 3) to stabilize their thermal expansion characteristics prior to tensile or thermal expansion testing. Specimens which received these treatments were designated "processed," and all other specimens which did not undergo these treatments were designated "as fabricated."

Experimental Procedures

Thermal cycling. Specimens from both the processed and as-fabricated specimen groups were thermally cycled between $-250°F$ and $250°F$ for up to 500 cycles. This temperature range is considered to represent the extremes the materials might experience in Earth orbit. The cycling was performed in a facility consisting of a hot chamber heated with electric resistance heaters and a cold chamber cooled with liquid nitrogen. The chambers are located side by side, separated by an insulating wall (fig. 3(a)). Each chamber contains two fans for rapid air circulation to minimize spatial temperature deviations. The specimens were automatically transferred from chamber to chamber in a sliding transfer compartment. A timer controlled the time the specimen rack remained in each chamber and the full cycle was recorded with a counter. A typical temperature profile, measured on a specimen instrumented with a chromel-alumel thermocouple, is shown in figure 3(b). A complete cycle lasted about 15 minutes, which included a period of approximately 5 minutes at both the maximum and minimum temperatures. The balance of the time (approximately 5 minutes) was required for the specimen temperature to come to equilibrium after transfers between chambers.

Thermal expansion. Thermal expansion measurements were made with a laser interferometric dilatometer specifically developed for measuring small thermal strains in composites (ref. 5). The strain resolution with the specimen geometry used in this study is approximately 1×10^{-6}. The thermal expansion test cycle for all specimens began by first heating each specimen from room temperature to the maximum test temperature, then cooling the specimen to the minimum temperature, and then heating the specimen to room temperature. One complete thermal expansion test cycle lasted about 18 hours. Thermal strain data were taken at approximately $40°F$ increments. There was a 30-minute hold at each temperature to allow the specimen and the dilatometer to reach thermal equilibrium. Expansion measurements were made over the temperature ranges of $-200°F$ to $200°F$ and $-250°F$ to $250°F$. Two temperature ranges were used to help define and understand the observed expansion behavior.

Tensile tests. Tensile properties were determined for both the as-fabricated and processed specimens before and after thermal cycling. At least three specimens were tested for each composite condition. All specimens were instrumented with back-to-back strain gages attached with a room-temperature adhesive. Testing was performed at room temperature with closed-loop servohydraulic test machines. The longitudinal and transverse specimens were tested at constant strain rates of 0.0010 per minute and 0.0013 per minute, respectively, until failure.

An automated data acquisition system was used to monitor and record specimen load, strain-gage output, and strain-gage bridge voltage. The system included a desktop computer, digital voltmeters, and a scanner. Tensile-test data were collected through the use of a computer program. A computer was also used for data reduction to provide stress-strain curves, ultimate strengths, and moduli.

Metallographic analyses. Representative as-fabricated and processed specimens, both before and after thermal cycling, were selected for metallographic analyses. Scanning electron microscope (SEM) examinations of the fracture surfaces were conducted to characterize the failure modes of the fibers, matrix, and surface foils. The SEM energy dispersive analysis of X-rays (EDAX) was used to investigate possible reactions between the matrix and fibers resulting from the thermal processing of the composite.

Microhardness measurement. Microhardness measurements in the surface foils of metallographically prepared laminate cross sections were used to assess the effects of processing and thermal cycling on the matrix elastic strength. The test procedure used was ASTM E 384—73, *The Standard Test Method for Microhardness of Materials* (ref. 6). Most microhardness measurements were made within the surface foils using a 15-g Knoop indenter. Only limited hardness measurements were made in the matrix because of interference with the graphite fibers. Increases in the microhardness of the surface foils on Gr/Al composites have been shown to correlate with reduced thermal strain hysteresis, which implies an increased matrix elastic strength (ref. 3). Reported microhardness values (in Knoop hardness number (KHN)) are averages of at least 10 separate measurements, each at random locations on the specimen.

Results and Discussion

Thermal Expansion and Microhardness

As-fabricated specimens. The thermal expansion behavior of as-fabricated P100 Gr/6061 Al composite specimens over the test temperature ranges investigated in this study is typically characterized by elastic and plastic deformations of the matrix alloy during thermal cycling. This results in thermal strain hysteresis and residual strain. The magnitude of the hysteresis depends upon the amount of plastic deformation during each cycle, which is directly related to the elastic limit of the matrix alloy. Figure 4 shows the thermal expansion of an as-fabricated diffusion-bonded P100 Gr/6061 Al composite during the first and second thermal expansion test cycles between −250°F and 250°F and after 500 thermal cycles between −250°F and 250°F. After the first thermal expansion test cycle, the as-fabricated composite shows a large residual strain (fig. 4(a)). This is attributed to a small plastic deformation during the initial heating from room temperature and a much larger plastic deformation during the subsequent cooling. The defor-

mations suggest that a larger thermal load is accommodated before compressive yielding (during heating) than that accommodated before tensile yielding (during cooling). This implies that a high residual tensile stress is present after fabrication. If the residual fabrication stress were zero, then the plastic deformations associated with heating and cooling from the median temperature of the thermal cycle would be equal, and therefore no residual strain would exist after the first thermal expansion test cycle. This unbalanced plastic deformation in tension and compression during the first thermal expansion cycle reduces the residual fabrication stress in the as-fabricated composite to about zero at the median temperature. As a result, the second thermal expansion test cycle (fig. 4(b)) over the same temperature range shows no additional residual dimensional changes. Therefore, an equal partitioning of the matrix elastic range is brought about by the first thermal expansion cycle, so that the plastic deformation in compression (during heating) is offset by the plastic deformation in tension (during cooling), resulting in zero residual strain.

Figure 4(c) shows a reduction in the magnitude of thermal strain hysteresis after 500 cycles compared with that which occurs during the second thermal expansion test cycle. This indicates that the matrix elastic range has increased with thermal cycling. The most likely cause for this increase is the continued aging and strain hardening of the matrix during thermal cycling.

An increase in the matrix elastic range also affects the average coefficient of thermal expansion (CTE) in the longitudinal direction (table I). These values are calculated from the thermal strains ϵ at the maximum and minimum temperatures T_{max} and T_{min} as follows:

$$CTE = \frac{\epsilon_{T,max} - \epsilon_{T,min}}{T_{max} - T_{min}}$$

The CTE's for the as-fabricated diffusion-bonded and hot-roll-bonded composite specimens are 0.23×10^{-6} per °F and 0.16×10^{-6} per °F, respectively, for their first thermal expansion test cycle between −250°F and 250°F. For the second thermal expansion test cycle, the CTE for the as-fabricated diffusion-bonded composite is larger (0.50×10^{-6} per °F) because of the reduction of the residual fabrication stress during the first thermal expansion test cycle. After 500 thermal cycles, the CTE for the diffusion-bonded composite is about 0.94×10^{-6} per °F, about two times greater than that for the second cycle, with a significantly reduced thermal strain

3

hysteresis. (The hot-roll-bonded composite could not be similarly tested because of insufficient material; however, similar changes would be expected.) The increase in CTE and decrease in the magnitude of hysteresis is the result of an increase in the elastic range of the matrix by thermal aging during thermal cycling. This reduces the plastic deformations which occur during thermal cycling, resulting in a smaller thermal strain hysteresis. The reduced plastic deformations also increase the importance of the matrix CTE and decrease the dominance of the fiber negative CTE, and hence the composite CTE becomes larger.

The effects of thermal cycling on the thermal expansion behavior of the as-fabricated P100 Gr/6061 Al composites (fig. 4) are consistent with changes in their microhardnesses (fig. 5). In this study, the elastic limit of the matrix is assumed to vary with the hardness in the same manner as the ultimate tensile strength varies with the hardness (fig. 6, from ref. 7). The increases in microhardness reflect the increases in elastic limit which resulted in a higher composite CTE and a lower thermal strain hysteresis with thermal cycling. The hot-roll-bonded composite would respond in a similar manner.

The larger average CTE of P100 Gr/6061 Al composites after thermal cycling would initially appear to be adverse to their potential applications in dimensionally critical structures. The significant reduction in thermal strain hysteresis, however, helps to compensate for the larger average CTE, since the initial large strain hysteresis would have rendered these materials totally unacceptable for use in space structures. The potential for microstructural changes to occur through metallurgical aging during the elevated-temperature portion of each thermal cycle is of concern since it could lead to increased thermal strain hysteresis if the elastic limit of the matrix is lowered by overaging.

Processed specimens. The thermal expansion behavior of processed P100 Gr/6061 Al composite specimens is typically characterized by a small thermal strain hysteresis, with little or no residual dimensional changes. Figures 7 and 8 show typical thermal expansion behaviors over two temperature ranges for processed diffusion-bonded and hot-roll-bonded composite specimens, respectively, before and after thermal cycling between $-250°F$ and $250°F$. The magnitude of the thermal strain hysteresis in figures 7(c) and 8(c) is significantly smaller than the hysteresis in the as-fabricated condition (fig. 4(b)). The hysteresis over the two temperature ranges used for the expansion measurements ($-200°F$ to $200°F$ and $-250°F$ to $250°F$) is not eliminated by processing

(figs. 7(a), 7(c), 8(a), and 8(c)). Plastic deformation occurs even though the nominal elastic limit of heat-treated 6061 aluminum is larger than the estimated maximum thermal stresses generated during thermal cycling between $-250°F$ and $250°F$, as discussed in reference 4. The hysteresis is not eliminated because the concentration of the alloying constituents important to the precipitation hardening of the matrix was below their specified levels, which results in a below nominal matrix strength (ref. 4).

Increasing the temperature range over which the expansion is measured by $100°F$ (from $-200°F$ to $200°F$ to $-250°F$ to $250°F$) increases the magnitude of thermal strain hysteresis and reduces the average CTE in both specimen groups (figs. 7(a), 7(c), 8(a), and 8(c), and table II). These differences are expected because of the increased amount of plastic deformation resulting from the larger thermal strains associated with the higher temperature range.

The thermal expansion behavior of the hot-roll-bonded and diffusion-bonded composites between $-200°F$ and $200°F$ and between $-250°F$ and $250°F$ is qualitatively very similar, both before and after thermal cycling. This indicates that the same mechanisms are active in both materials, with the difference in the magnitudes of hysteresis attributed to the difference in the elastic limits of each matrix. There are no significant differences between the expansion behavior of the diffusion-bonded composites before and after thermal cycling for either temperature range (compare figs. 7(a) and 7(b) and figs. 7(c) and 7(d)). The same is true for the hot-roll-bonded composites (figs. 8(a) to 8(d)).

The average CTE of the processed composites between $-200°F$ and $200°F$ and between $-250°F$ and $250°F$ before and after thermal cycling are shown in figure 9 and table II. The CTE of the diffusion-bonded composite between $-200°F$ and $200°F$ and between $-250°F$ and $250°F$ and the CTE of the hot-roll-bonded composite between $-200°F$ and $200°F$ do not significantly change after 500 thermal cycles. The data indicate that the CTE of the hot-roll-bonded composite between $-250°F$ and $250°F$ decreases slightly. In general, no significant changes in the elastic range with thermal cycling are indicated. This is consistent with the microhardness measurements shown in figure 10, which do not show any significant changes in the hardness (elastic limit) of either processed diffusion-bonded or hot-roll-bonded composites after 500 thermal cycles.

Any reductions in CTE would indicate an increase in the plastic deformation of the matrix because of a decrease in the elastic limit of the matrix. Since the CTE (fig. 9) and the microhardness (fig. 10) do not significantly change after 500 thermal cycles, the

4

matrix properties after processing may be considered more stable than for as-fabricated composites. It should be pointed out, however, that 500 thermal cycles as performed in this study translates to a total of only about 42 hours at the maximum temperature. Also, thermal control coatings may be used to keep the temperature below 250°F. Since a 10-year application would amount to 5 years, or about 43 800 hr, at the maximum temperature in Earth orbit, much work is still needed to assess the long-term stability of the thermal expansion behavior of P100 Gr/6061 Al composites.

Tensile Properties

Diffusion-bonded composites—longitudinal properties. Typical longitudinal tensile stress-strain curves for as-fabricated and processed diffusion-bonded composites before thermal cycling are shown in figure 11. Each curve is bilinear, typical of Gr/Al composites (ref. 8), with the regions referred to as stage I and stage II. These regions are separated by the stage I-to-stage II transition point marked on each curve. These transition points are located at the point of initial deviation from the linear stage I behavior. The stage I-to-stage II transition stress is between 60 ksi to 70 ksi for the as-fabricated composites. The transition stress is generally within 5 ksi of the ultimate tensile strength (UTS) for the thermally cycled composites and for all processed composites. The increase in the transition stress from cycling or processing can be attributed to the increase in the elastic limit of the matrix by either the heat treatment or the aging during thermal cycling and by the reduction of the residual tensile fabrication stresses by the cryogenic stress relief of the first thermal cycle.

The longitudinal UTS and tensile modulus values for the as-fabricated and processed composites as a function of the number of thermal cycles are given in table III and figure 12. Each data point of figure 12 is the average of three tests, and curves have been faired through the data averages for a particular composite condition. The large standard deviation bars shown in figure 12(a) indicate a high amount of variability to the UTS data. This may suggest a highly nonuniform bonding within the composites fabricated through diffusion bonding. The average UTS of the as-fabricated specimens increases by about 13 percent after 100 thermal cycles but does not significantly change with further cycling up to 500 cycles, as shown in figure 12(a). This is consistent with the metallurgical aging of these specimens during the high-temperature end of each thermal cycle, which strengthened the matrix. The uncycled processed specimens showed a higher UTS than the uncycled

as-fabricated specimens (by about 18 percent), and this UTS did not significantly change with thermal cycling.

Before thermal cycling, the processed specimens show a stage I modulus about 9 percent higher than that of the as-fabricated specimens (fig. 12(b)). The modulus of the processed specimens is not affected by thermal cycling. After 100 thermal cycles, the as-fabricated specimens attain about the same average stage I modulus as the processed specimens, and the modulus remains essentially unchanged with further cycling. The increase in the stage I modulus of the as-fabricated composites with thermal cycling or processing cannot be reasonably attributed to an increase in the modulus or the work hardening coefficient of the metal-matrix alloy, since the Young's modulus of aluminum alloys is considered independent of the metallurgical temper. A possible reason for this higher modulus could be a straightening of fibers during plastic deformation of the matrix, which would increase the number of load-carrying fibers. However, the real mechanism responsible for the observed increase in modulus is not understood.

The strain at failure for the diffusion-bonded specimens is also presented in table III. The small changes in the strain at failure as a result of thermal cycling and processing are consistent with those expected based upon the observed changes in the UTS and modulus. For example, if the modulus remains constant, any increase in the UTS would be accompanied by an increase in the strain at failure of about the amount predicted by Hooke's law.

Typical fracture profiles of the diffusion-bonded composite specimens are shown in figure 13(a), and representative SEM fractographs are shown in figure 13(b). The fracture profiles and surface morphologies of the specimens show no indication of a change in the fracture mode as a result of thermal cycling or thermal processing. All failures are characterized by ductile necking of the face sheets and the matrix alloy and by brittle fracture of the graphite fibers. Fiber pullout is evident in all fractures, indicating a weak bond between the graphite fibers and the aluminum matrix in both the as-fabricated and processed composites. The SEM EDAX examinations of fracture surfaces show no evidence of any reaction between the graphite fibers and the aluminum matrix in any of the composites.

Diffusion-bonded composites—transverse properties. Typical transverse tensile stress-strain behavior of as-fabricated and processed diffusion-bonded composite specimens, before and after thermal cycling, is shown in figure 14. Ultimate tensile strength and modulus data are given in table IV. The specimens

for transverse tensile tests had a residual curvature along their transverse direction as a result of fabrication. This curvature caused through-the-thickness stress gradients to develop during the initial tensile loading which straightened the specimen. Since these stress gradients affect the measured properties, these data are presented for completeness and caution must be used in their interpretation.

The transverse tensile specimens show continuous plastic yielding until failure at stresses of less than 4 ksi. The tensile loads at which both the as-fabricated and processed composites fail are less than those which should easily be supported by only the cross-sectional area of the aluminum face sheets themselves. These low strengths may be related to the through-the-thickness stress gradient.

Typical fracture profiles of the as-fabricated and processed composite specimens are shown in figure 15(a). Typical high-magnification SEM fractographs are shown in figure 15(b). These fracture profiles and fracture morphologies indicate no change in the failure modes from either thermal cycling or thermal processing. Specimen fractures are characterized by ductile necking of the foil face sheets with partial delamination at the diffusion bond line between the face sheets and the composite tows. Clean separation of the graphite fibers from the aluminum matrix is also observed, with all specimens indicating a weak graphite-matrix interfacial bond. This bond is not significantly changed by the thermal processing.

Hot-roll-bonded composites. Typical longitudinal tensile stress-strain curves of the as-fabricated and processed hot-roll-bonded composites are shown in figure 16. Each curve is bilinear, similar to those for the diffusion-bonded composites. The stage I-to-stage II transition stress is higher after processing, as was noted for the diffusion-bonded composites. There is not as much difference between curves for the as-fabricated and processed composites as there is for the diffusion-bonded composites (fig. 11). In general, the longitudinal tensile properties of the hot-roll-bonded composites (table V) are lower than those of the diffusion-bonded composites (table III). The variability of the UTS data for the hot-roll-bonded composites is higher than that observed for the diffusion-bonded composites. The UTS data for as-fabricated specimens have a range of 65 ksi for the hot-roll-bonded composites compared with 26 ksi for the diffusion-bonded composites. For processed specimens, the UTS data vary by about 28 ksi for the hot-roll-bonded composites and by about 15 ksi for the diffusion-bonded composites. The larger scatter in the UTS data for the hot-roll-bonded composites may

indicate that they are less uniformly bonded than the diffusion-bonded composites. However, since the data scatter in both composites is large, both fabrication techniques should be improved to provide more reproducible tensile properties.

The effects of thermal cycling on the stage I modulus and UTS are shown in figure 17 and in table V. The strain at failure data are also presented in table V. Each data point in figure 17 is the average of three tests and curves have been faired through each set of data. Because the data scatter is large (indicated by the standard deviation bars), no significant changes in the UTS and in the modulus of the hot-roll-bonded composites by thermal processing or thermal cycling can be inferred.

Typical fracture profiles of as-fabricated, processed, and thermally cycled processed composite specimens loaded in the fiber direction are shown in figure 18(a). These profiles are not smooth compared with those of the diffusion-bonded composite specimens (fig. 13(a)). These profiles, together with the larger scatter in the tensile data for the hot-roll-bonded composites, may indicate a poorer uniformity in bonding throughout the hot-roll-bonded composites compared with the diffusion-bonded composites. This may account for the generally lower strength of the hot-roll-bonded composites. The SEM fractographs of the hot-roll-bonded composites are shown in figure 18(b). The fracture profiles and surface morphology of these specimens do not indicate any significant changes in the failure mode as a result of processing or thermal cycling of the processed specimens. The failures are characterized by ductile necking of the face sheets and the matrix alloy, with brittle fracture of the graphite fibers similar to that observed in the diffusion-bonded composites. Fiber pullout is also evident in all fractures. High-magnification SEM EDAX examinations show no evidence of any reaction between the graphite fibers and the matrix resulting from the thermal processing.

Concluding Remarks

The effects of thermal cycling on the thermal expansion behavior and mechanical properties of Thornel P100 graphite fiber/6061 aluminum (P100 Gr/6061 Al) composites, as fabricated and after processing to eliminate thermal strain hysteresis, have been investigated. Two groups of composites were studied: one was fabricated by hot roll bonding and the other by diffusion bonding. The effects of thermal processing and thermal cycling on the thermal expansion and mechanical properties can be summarized as follows:

The first thermal cycle of the as-fabricated diffusion-bonded composite resulted in considerable

residual strain. This cycle reduces the residual fabrication stress to about zero at the median temperature of the cycle. This was inferred by the absence of residual strains after further cycling over the same temperature range and indicated an equal partitioning of the matrix elastic range, so that at temperatures greater than the median temperature the matrix is under compressive thermally induced loads and at temperatures less than the median temperature the matrix is under tensile thermally induced loads.

Thermal cycling of as-fabricated diffusion-bonded P100 Gr/6061 Al composites improved the tensile strength and stiffness and reduced the thermal strain hysteresis. An increase in the average coefficient of thermal expansion accompanied the reduced hysteresis. This was attributed to aging of the aluminum matrix alloy during thermal cycling.

The processed diffusion-bonded and hot-roll-bonded composites exhibited significantly reduced thermal strain hysteresis from that of the as-fabricated composites. The thermal processing of the diffusion-bonded composites significantly increased their strength and stiffness. Scatter in the data obscured any effects of thermal processing on the mechanical properties of the roll bonded composites.

The thermal expansion behavior of the processed composites was not significantly affected by thermal cycling. In both the processed diffusion-bonded and hot-roll-bonded composites, the large scatter in the data (because of material variability) may have prevented the observation of any effects of thermal cycling on mechanical properties.

In general, the processed diffusion-bonded composites were stronger and stiffer than the processed hot-roll-bonded composites and exhibited much more uniform fracture profiles. The diffusion-bonded composites may therefore have been more uniformly bonded than the hot-roll-bonded composites. The scatter in the mechanical property data was significant in both the hot-roll-bonded and diffusion-bonded composites, but was greater with the hot-roll-bonded composites. The large scatter in the data indicates the need to improve composite fabrication techniques to provide more reproducible properties.

The importance of the metallurgical condition of the composite matrix to composite properties requires that the effects of thermal cycling of the Al matrix properties be more closely examined. The strengthening of the matrix in the as-fabricated composites by metallurgical aging during thermal cycling shows a potential for aging during prolonged exposure in Earth orbit if the temperature extremes reach -250°F to 250°F. If the elastic limit of the matrix is lowered by overaging, thermal stability and mechanical properties could be degraded.

References

1. Tenney, Darrel R.; Sykes, George F.; and Bowles, David E.: Space Environmental Effects on Materials. *Environmental Effects on Materials for Space Applications*, AGARD-CP-327, Mar. 1983, pp. 6-1-6-24.
2. Min, B. K.; and Crossman, F. W.: History-Dependent Thermomechanical Properties of Graphite/Aluminum Unidirectional Composites. *Composite Materials: Testing and Design (Sixth Conference)*, I. M. Daniel, ed., ASTM STP 787, 1982, pp. 371-392.
3. Dries, Gregory A.; and Tompkins, Stephen S.: *Thermal Processing of Graphite-Reinforced Aluminum To Minimize Thermal Strain Hysteresis*. NASA TP-2402, 1985.
4. Dries, Gregory A.; and Tompkins, Stephen S.: *The Effect of Matrix Chemistry on the Thermal Expansion Behavior Of Graphite/Aluminum Composites*. NASA TM-86445, 1985.
5. Tompkins, Stephen S.; Bowles, David E.; and Kennedy, William R.: A Laser-Interferometric Dilatometer for Thermal-Expansion Measurements of Composites. Exp. Mech., vol. 26, no. 1, Mar. 1986, pp. 1-6.
6. *Standard Test Method for Microhardness of Materials*. ASTM Designation: E 384—73 (Reapproved 1979). Part 11 of 1982 Annual Book of ASTM Standards, c.1982, pp. 373-393.
7. *Metals Handbook*®, Ninth ed. Volume 4—Heat Treating. American Soc. Metals, c.1981.
8. Kreider, Kenneth G., ed.: *Metallic Matrix Composites*. Academic Press, Inc., c.1974.

Table I. Effects of Thermal Cycling on CTE of As-Fabricated Composites

Fabrication process	Number of thermal cycles	CTE, per °F, for temperature range of —	
		$-200°F$ to $200°F$	$-250°F$ to $250°F$
Diffusion bonding	1	0.38×10^{-6}	0.23×10^{-6}
	2		0.50×10^{-6}
	500		0.86×10^{-6} 1.02
	Average . . .		0.94×10^{-6}
Hot roll bonding	1		0.16×10^{-6}

Table II. Effects of Thermal Cycling on CTE of Processed Composites

Fabrication process	Number of thermal cycles	CTE, per °F, for temperature range of —	
		$-200°F$ to $200°F$	$-250°F$ to $250°F$
Diffusion bonding	1	0.72×10^{-6} .67 .73	0.59×10^{-6}
	Average . . .	0.71×10^{-6}	0.59×10^{-6}
	100	0.80×10^{-6} .71 .76	
	Average . . .	0.76×10^{-6}	
	500	0.69×10^{-6} .79 .70	0.59×10^{-6}
	Average . . .	0.73×10^{-6}	0.59×10^{-6}
Hot roll bonding	1	1.06×10^{-6} .79	1.04×10^{-6} .75
	Average . . .	0.93×10^{-6}	0.90×10^{-6}
	100	0.93×10^{-6}	
	500	0.84×10^{-6} .83	0.66×10^{-6}
	Average . . .	0.84×10^{-6}	0.66×10^{-6}

Table III. Room-Temperature Longitudinal Tensile Properties
of Diffusion-Bonded Composite

Number of cycles between −250°F and 250°F	As-fabricated composite values of—				Processed composite values of—		
	Ultimate tensile strength, ksi	Strain,* percent	Stage I modulus, psi	Stage II modulus, psi	Ultimate tensile strength, ksi	Strain,* percent	Stage I modulus, psi
0	90.0	0.214	41.9×10^{-6}	39.5×10^{-6}	125.3	0.248	48.9×10^{-6}
	106.9	.252	44.0	42.1	114.1	.232	47.7
	116.4	.251	48.4	43.5	129.1	.258	49.5
Average . . .	104.4	0.239	44.8×10^{-6}	41.7×10^{-6}	122.8	0.246	48.7×10^{-6}
100	122.2	0.235	51.4×10^{-6}		108.9	0.220	49.1×10^{-6}
	117.4	.227	50.4		129.9	.264	48.5
	110.8	.252	42.8		133.8	.265	49.9
	120.3	.237	50.4				
Average . . .	117.7	0.238	48.7×10^{-6}		124.2	0.250	49.2×10^{-6}
500	110.0	0.223	48.1×10^{-6}		112.8	0.233	48.1
	114.1	.223	50.4		123.9	.245	49.9
	114.3	.217	51.8		123.0	.248	49.0
	113.8	.224	50.6				
Average . . .	113.1	0.222	50.2×10^{-6}		119.9	0.242	49.0×10^{-6}

*Percent strain at failure, from strain-gage output.

Table IV. Room-Temperature Transverse Tensile Properties of Thermally
Cycled Diffusion-Bonded Composite Specimens

Number of cycles between $-250°$F and $250°$F	As-fabricated composite values of—		Processed composite values of—	
	Ultimate tensile strength, ksi	Modulus,* psi	Ultimate tensile strength, ksi	Modulus,* psi
0	3.2	3.13×10^6	2.0	2.59×10^6
	†1.3		†.5	
	1.9	4.01	1.6	2.48
	2.6	2.96		
Average . . .	2.6	3.37×10^6	1.8	2.54×10^6
100	3.6	3.70×10^6		
500	†0.8		1.8	3.17×10^6
	3.6	3.54×10^6	1.6	2.87
	3.5	3.25		
Average . . .	3.6	3.39×10^6	1.7	3.02×10^6

*Secant modulus at strain of 0.04 percent.
†Not included in average.

Table V. Room-Temperature Longitudinal Tensile Properties of
Thermally Cycled Hot-Roll-Bonded Composite Specimens

Number of cycles between −250°F and 250°F	As-fabricated composite values of—				Processed composite values of—		
	Ultimate tensile strength, ksi	Strain,* percent	Stage I modulus, psi	Stage II modulus, psi	Ultimate tensile strength, ksi	Strain,* percent	Stage I modulus, psi
0	93.0	0.222	44.3×10^6	39.2×10^6	98.2	0.226	44.2×10^6
	†49.0		44.1		105.9	.242	43.7
	†28.2		39.6		77.7	.161	44.3
	†52.0	.202	39.7				
	79.1	.188	42.0	39.1×10^6			
Average . . .	86.1	0.204	41.9×10^6	39.2×10^6	93.9	0.210	44.1×10^6
100					94.5	0.209	44.6×10^6
					73.1	.129	43.7
					*35.6		40.9
					77.3	.188	44.2
Average . . .					81.6	0.175	43.3×10^6
500					98.2	0.248	43.3×10^6
					80.3	.183	43.9
					†34.6		
					78.8	.199	41.8
Average . . .					85.8	0.210	43.0×10^6

*Percent strain at failure from strain-gage output.
†Not included in average.

11

(a) Diffusion bonded.

(b) Hot roll bonded.

L-84-12,924
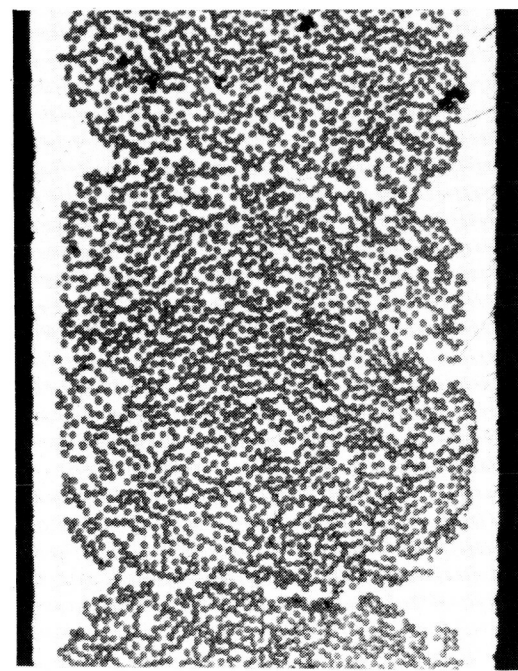
Figure 1. Optical micrographs of single-ply P100 Gr/6061 Al composites.

Fiberglass gripping tabs
bonded in place

Fiber orientation

0.025

0.188

2.0

2.0

2.0

0.5
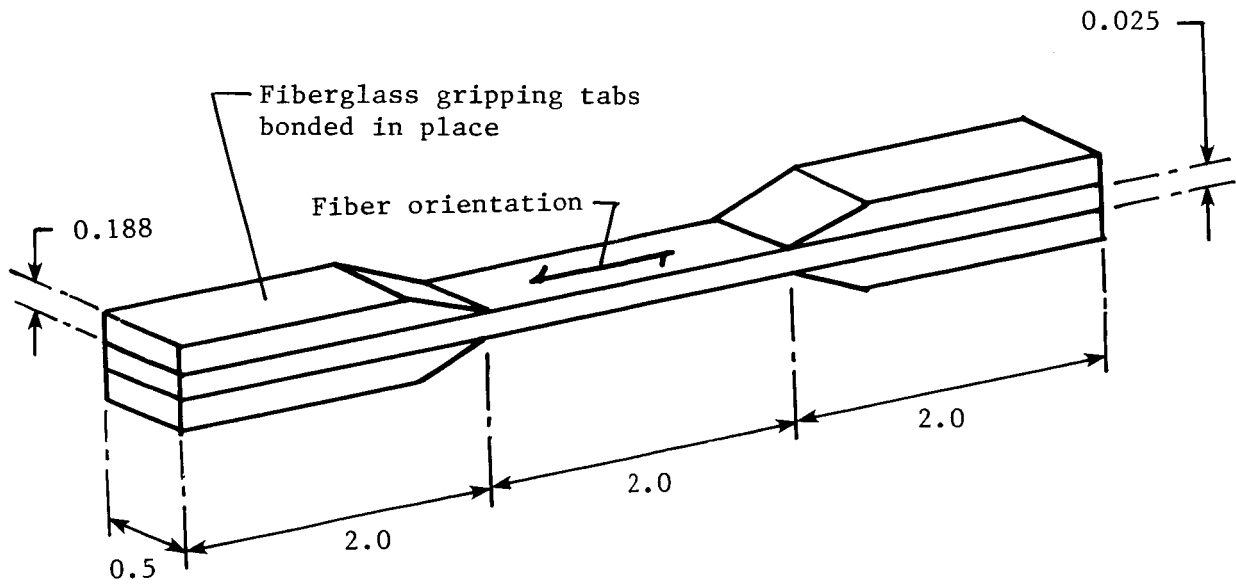
(a) Longitudinal tensile-test specimen.

0° fiber direction

1.000

3.017
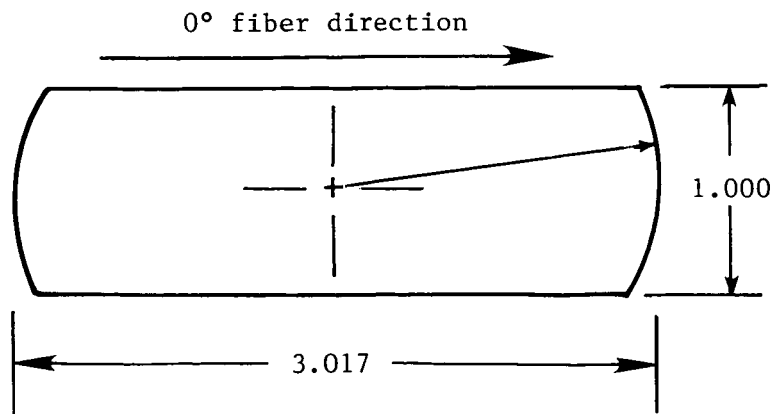
(b) Thermal expansion specimen.

Figure 2. Schematic diagrams of tensile-test and thermal expansion specimens. Dimensions in inches.
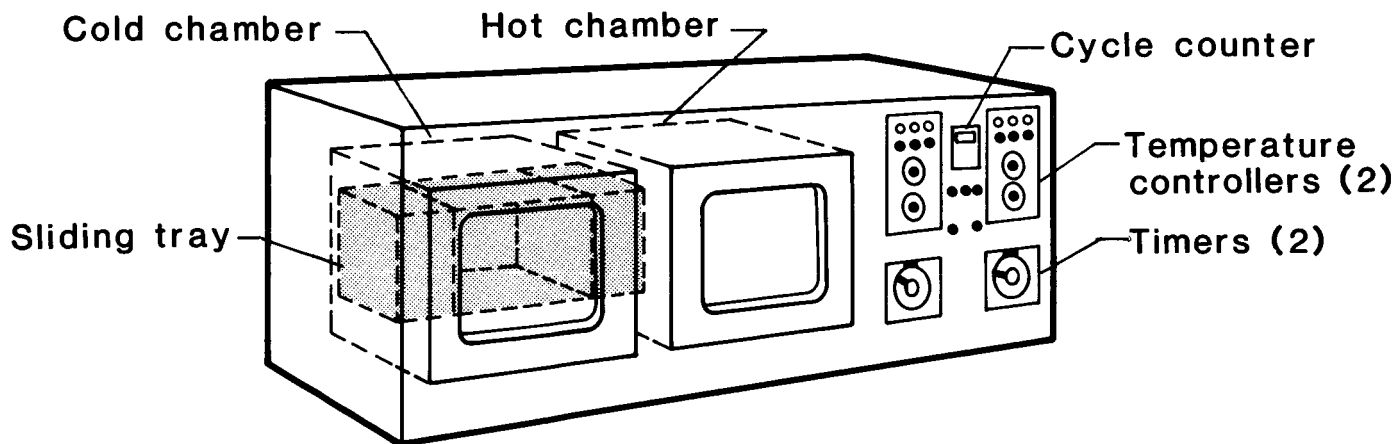
(a) Thermal cycling apparatus.
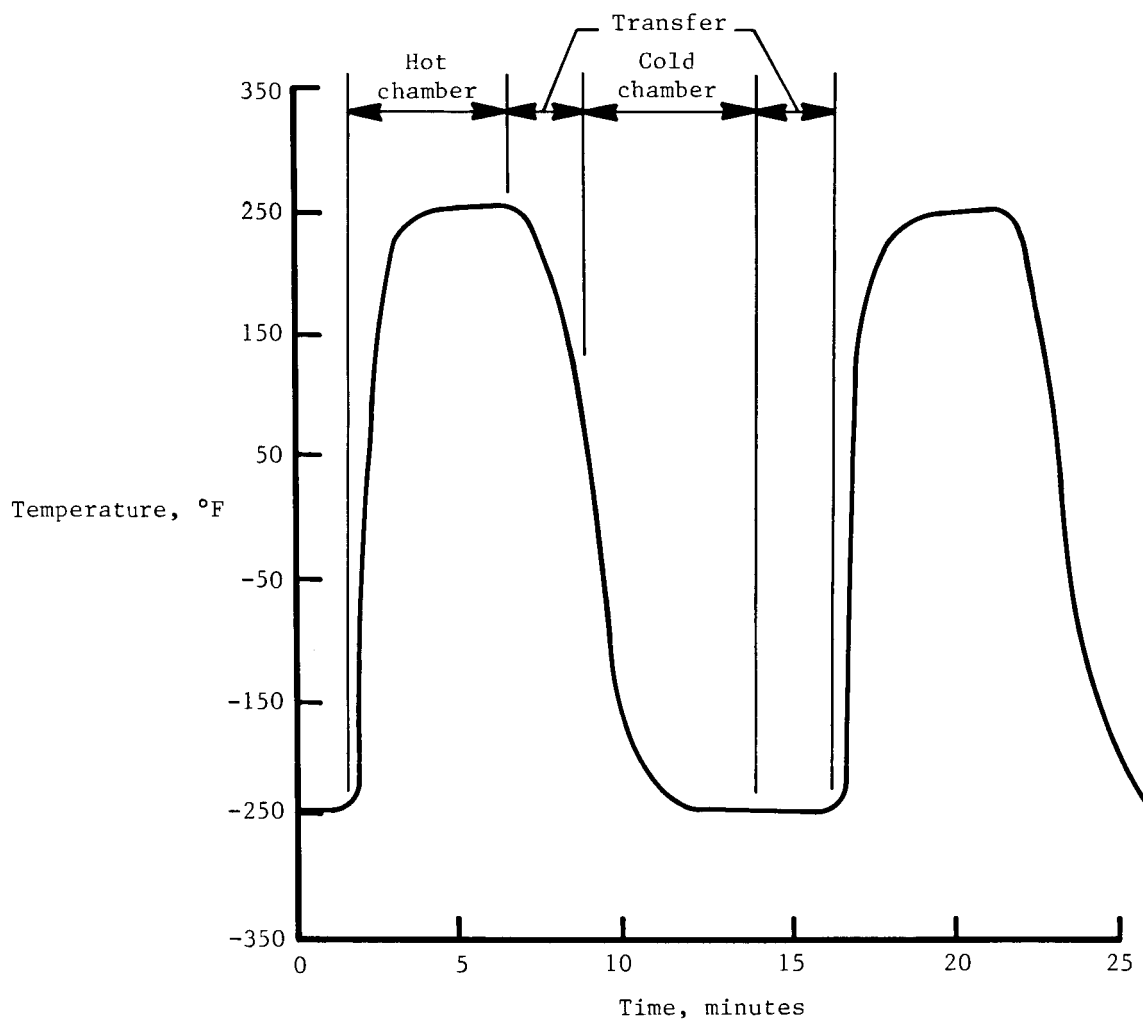
(b) Typical temperature profile.

Figure 3. Thermal cycling apparatus and typical temperature profile attained during thermal cycling.
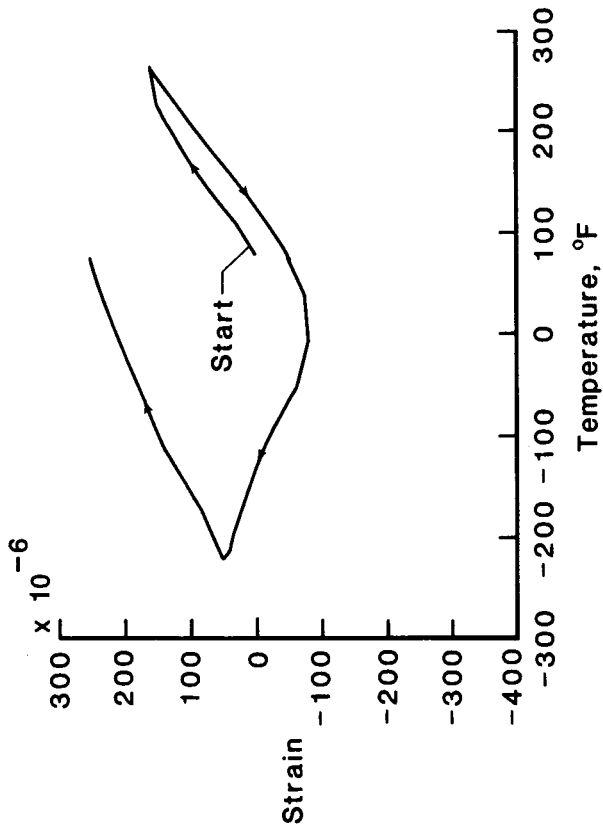
(a) First thermal expansion test cycle.
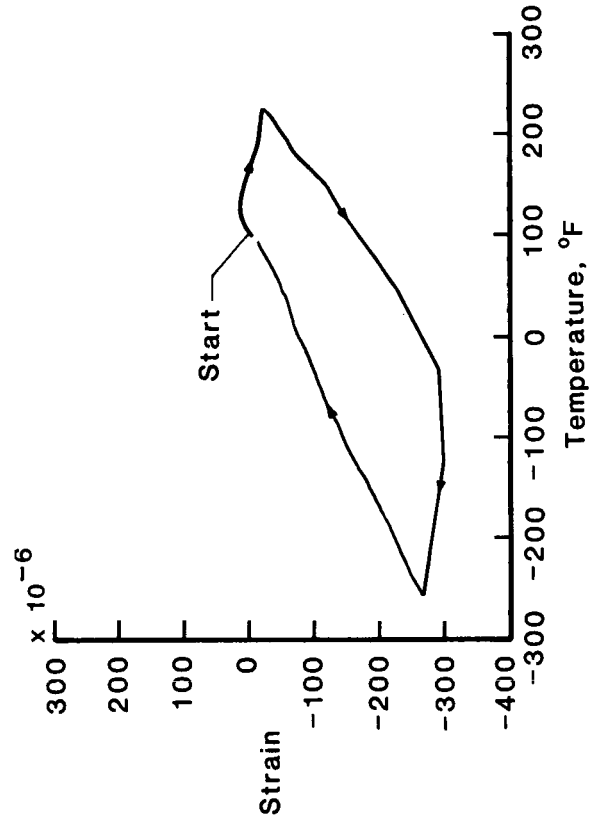
(b) Second thermal expansion test cycle.
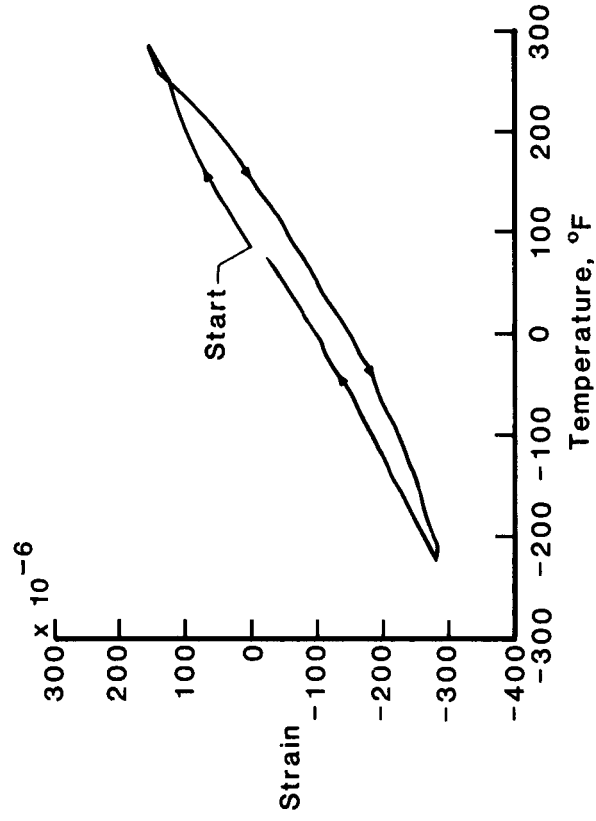
(c) Thermal expansion after 500 thermal cycles between −250°F and 250°F.

Figure 4. Thermal expansion behavior between −250°F and 250°F of as-fabricated diffusion-bonded P100 Gr/6061 Al composite.

15
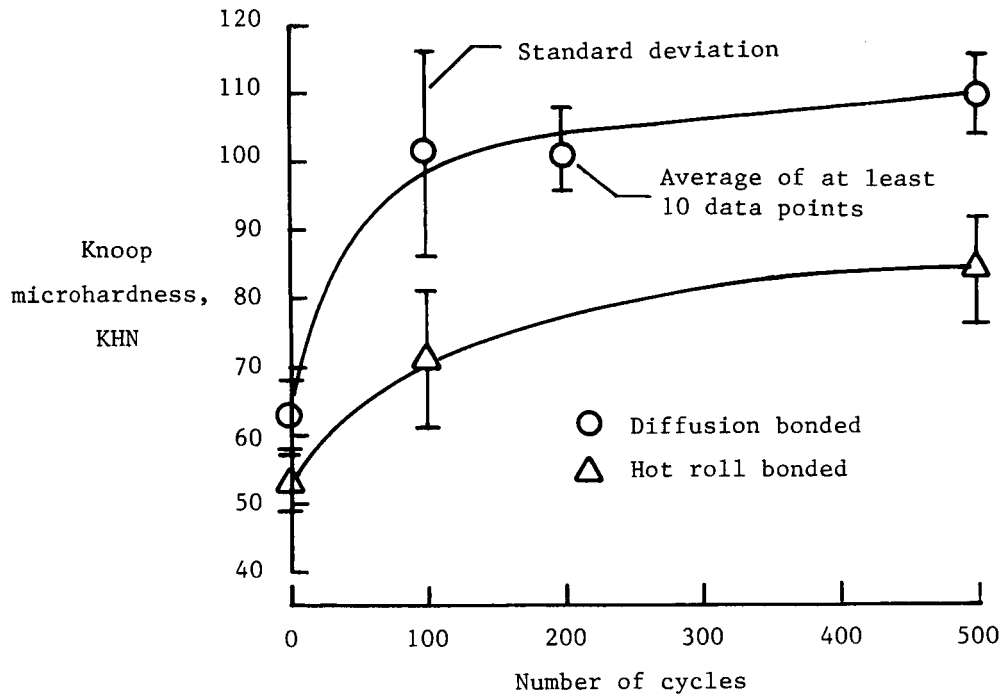
Figure 5. Effect of thermal cycling between −250°F and 250°F on microhardness of as-fabricated P100 Gr/6061 Al composites.
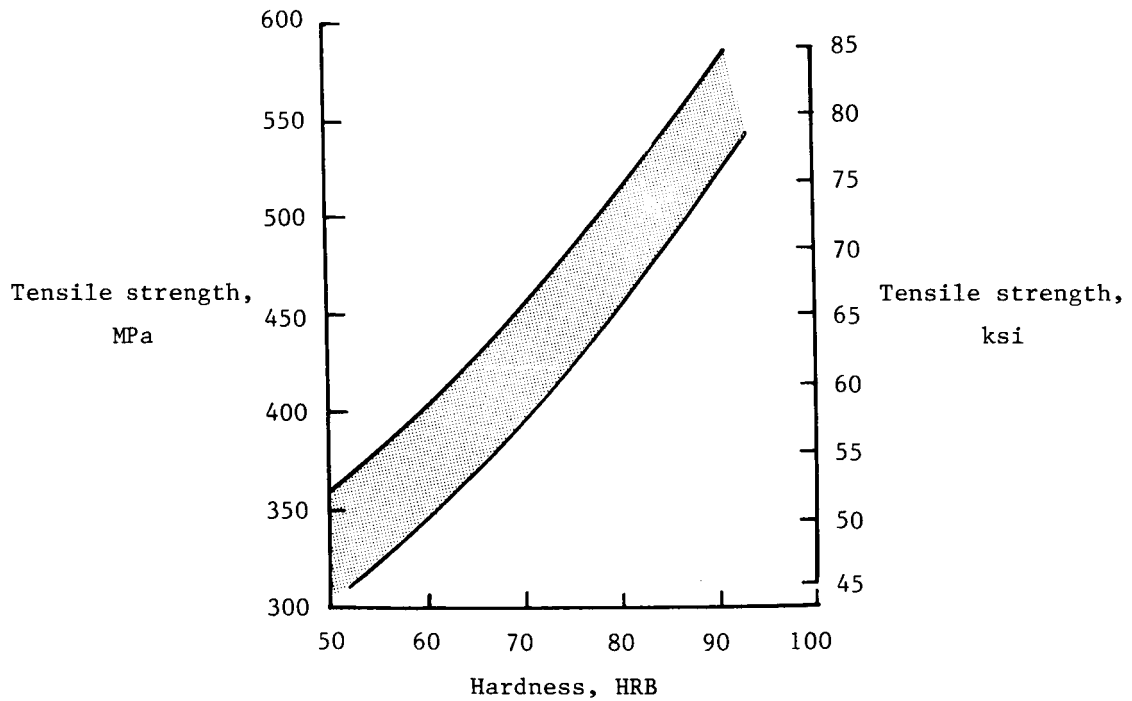
Figure 6. Tensile strength vs hardness for various aluminum alloys and tempers. (From p. 715, ref. 7.)
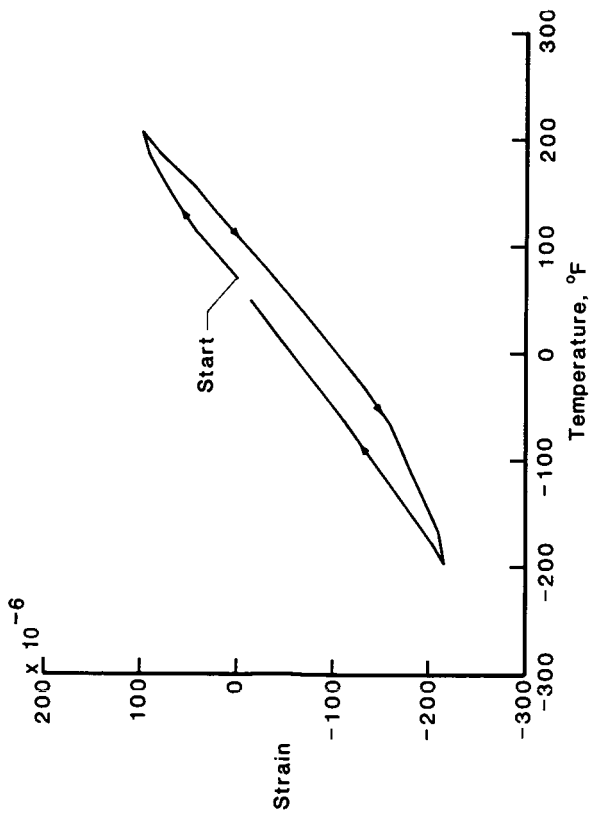
(a) First thermal expansion test cycle between −200°F and 200°F.
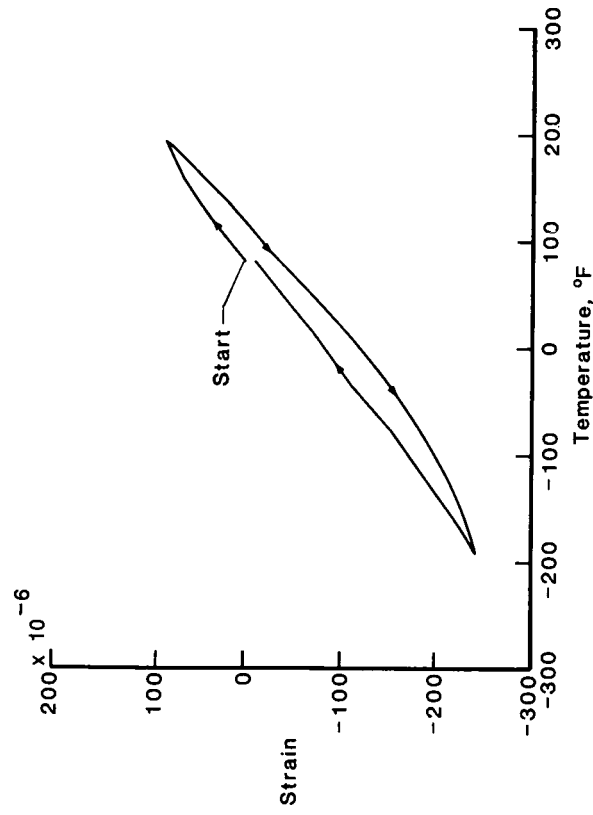
(b) Thermal expansion between −200°F and 200°F after 500 thermal cycles.
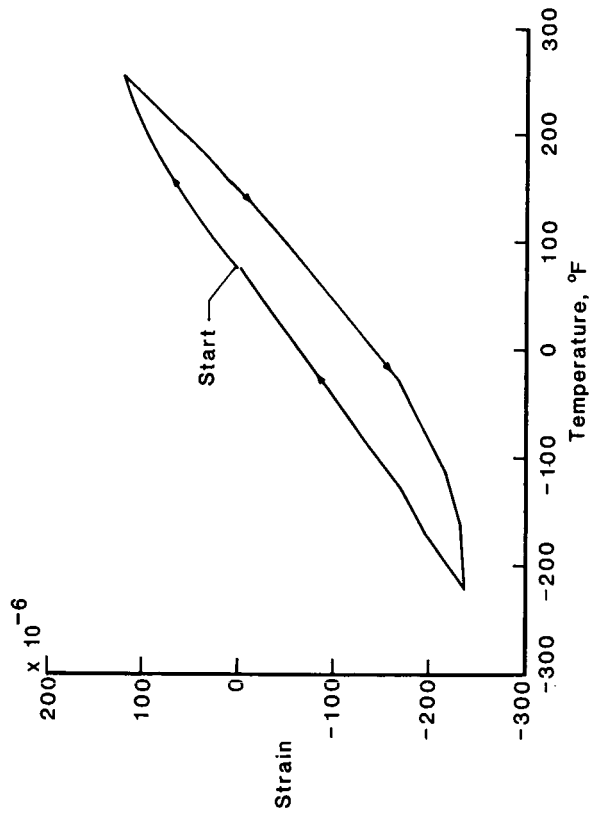
(c) First thermal expansion test cycle between −250°F and 250°F.
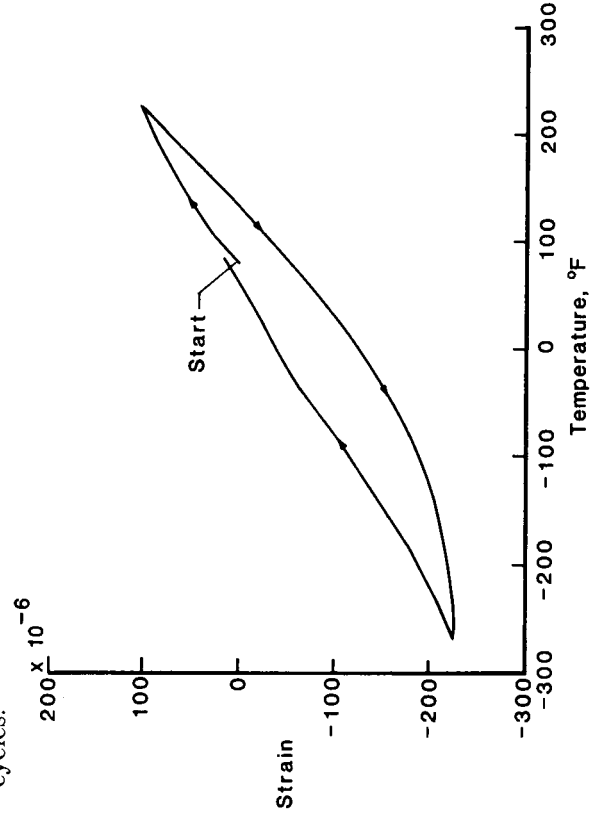
(d) Thermal expansion between −250°F and 250°F after 500 thermal cycles.

Figure 7. Thermal expansion behavior of processed diffusion-bonded P100 Gr/6061 Al composite specimens before and after thermal cycling between −250°F and 250°F.

17
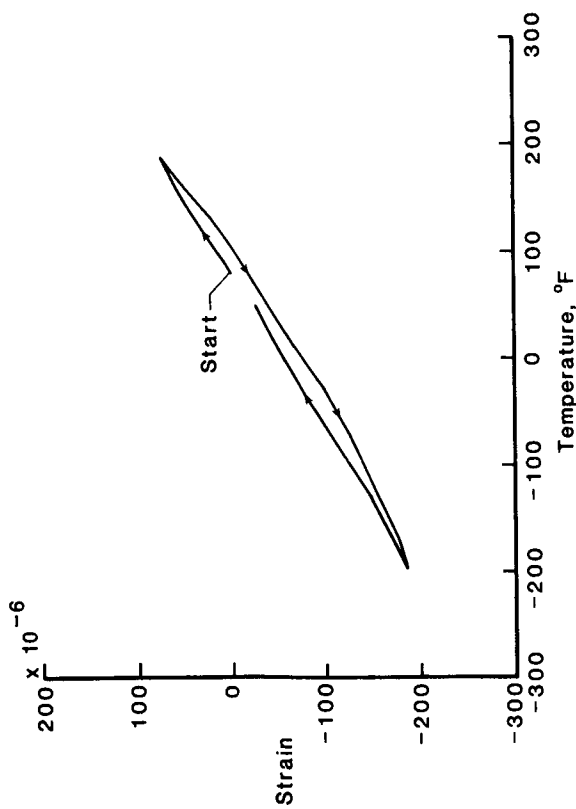
(a) First thermal expansion test cycle between −200°F and 200°F.
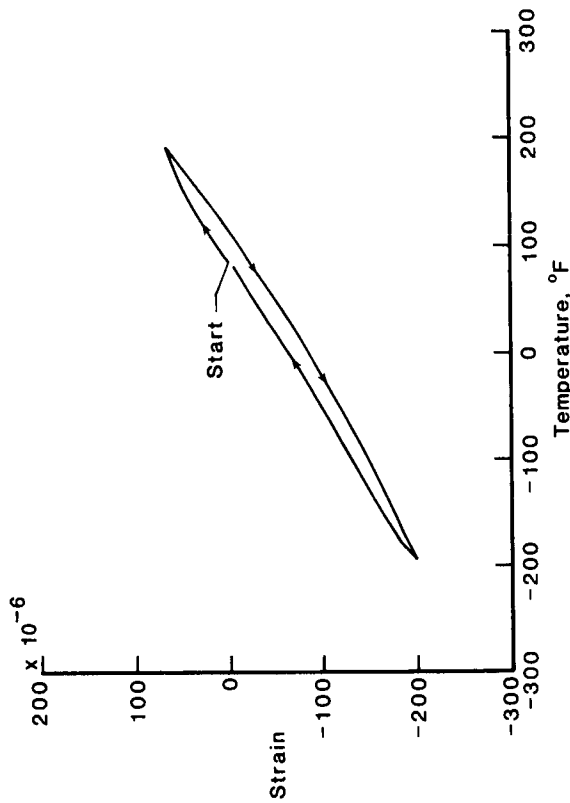
(b) Thermal expansion between −200°F and 200°F after 500 thermal cycles.
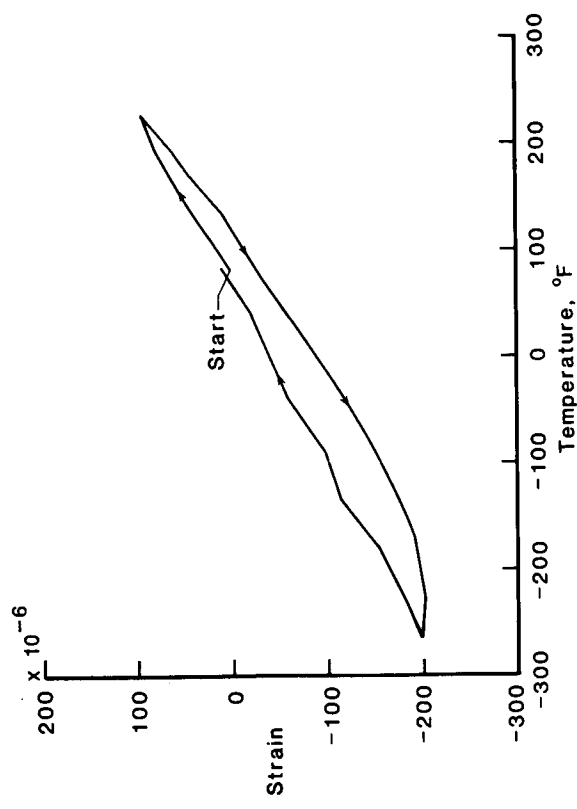
(c) First thermal expansion test cycle between −250°F and 250°F.
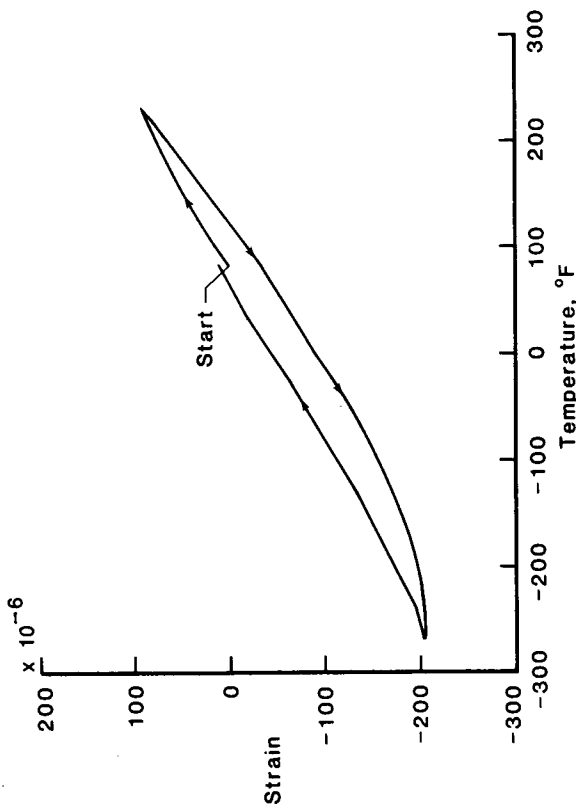
(d) Thermal expansion between −250°F and 250°F after 500 thermal cycles.

Figure 8. Thermal expansion behavior of processed hot-roll-bonded P100 Gr/6061 Al composite specimens before and after thermal cycling between −250°F and 250°F.
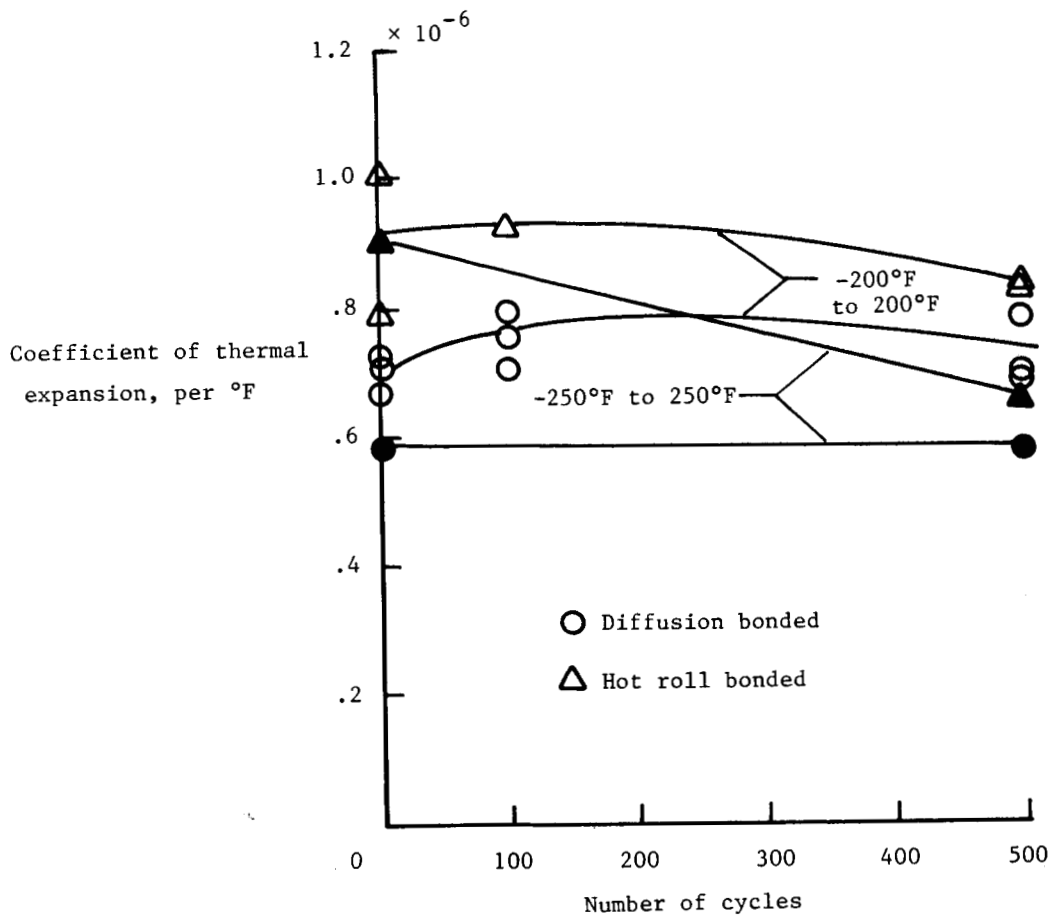
Figure 9. Effect of thermal cycling between −250°F and 250°F on CTE of processed P100 Gr/6061 Al composites.
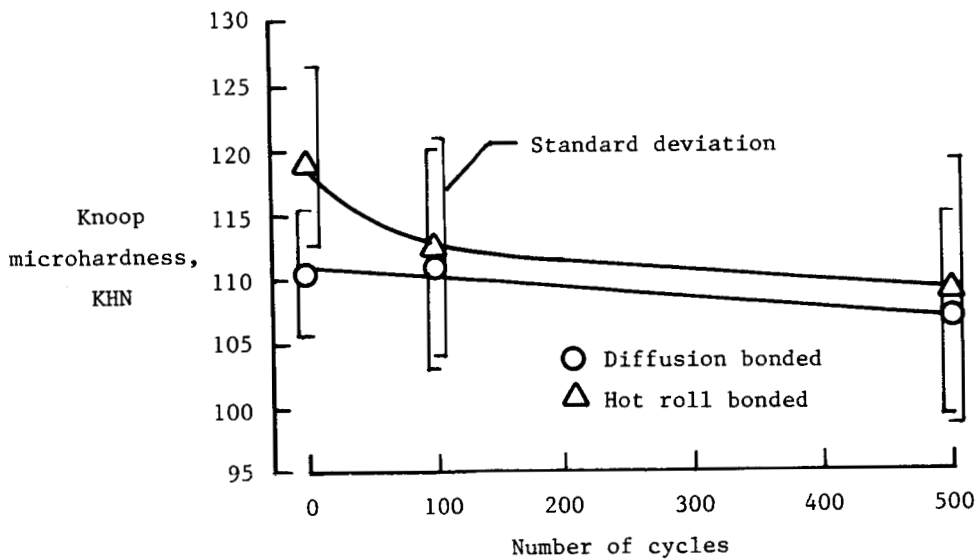
Figure 10. Effect of thermal cycling between −250°F and 250°F on microhardness of processed P100 Gr/6061 Al composites. Average of at least 10 data points.
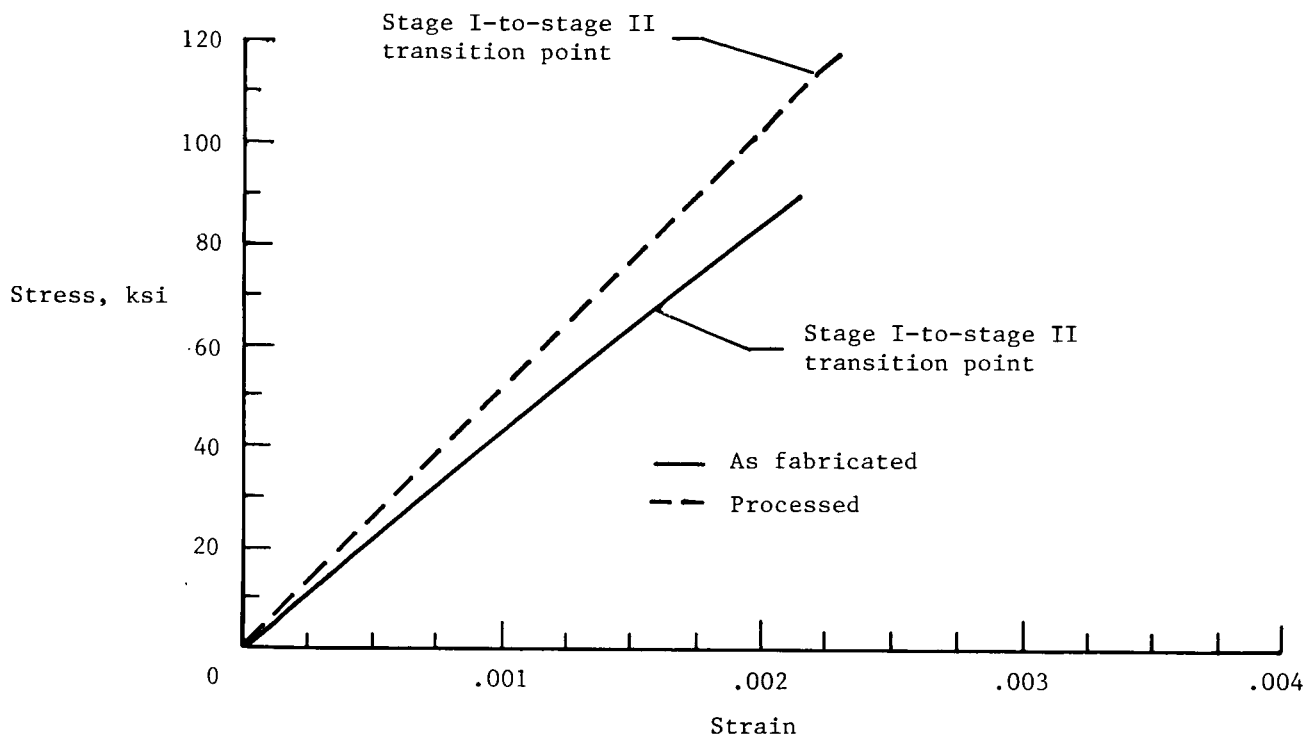
Figure 11. Typical longitudinal tensile stress-strain curves for diffusion-bonded P100 Gr/6061 Al composites.
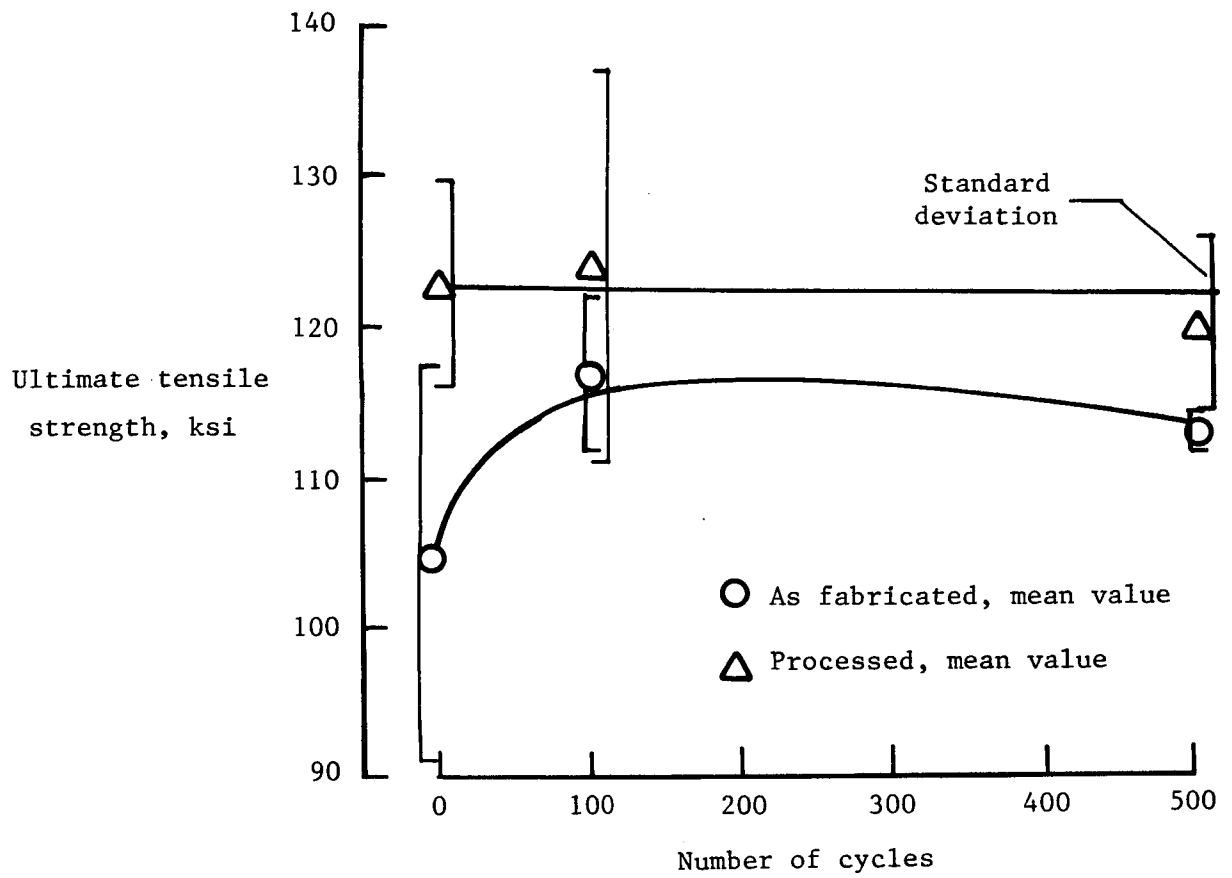
(a) Ultimate tensile strength.
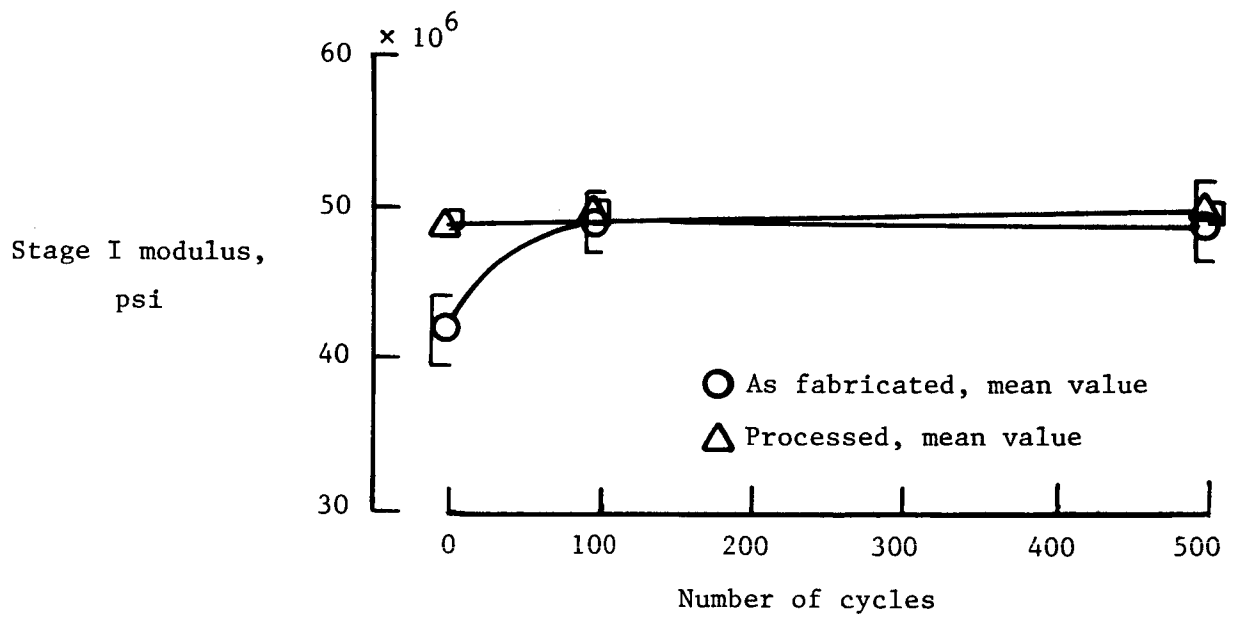
(b) Stage I modulus.

Figure 12. Longitudinal tensile properties for thermally cycled diffusion-bonded P100 Gr/6061 Al composites.
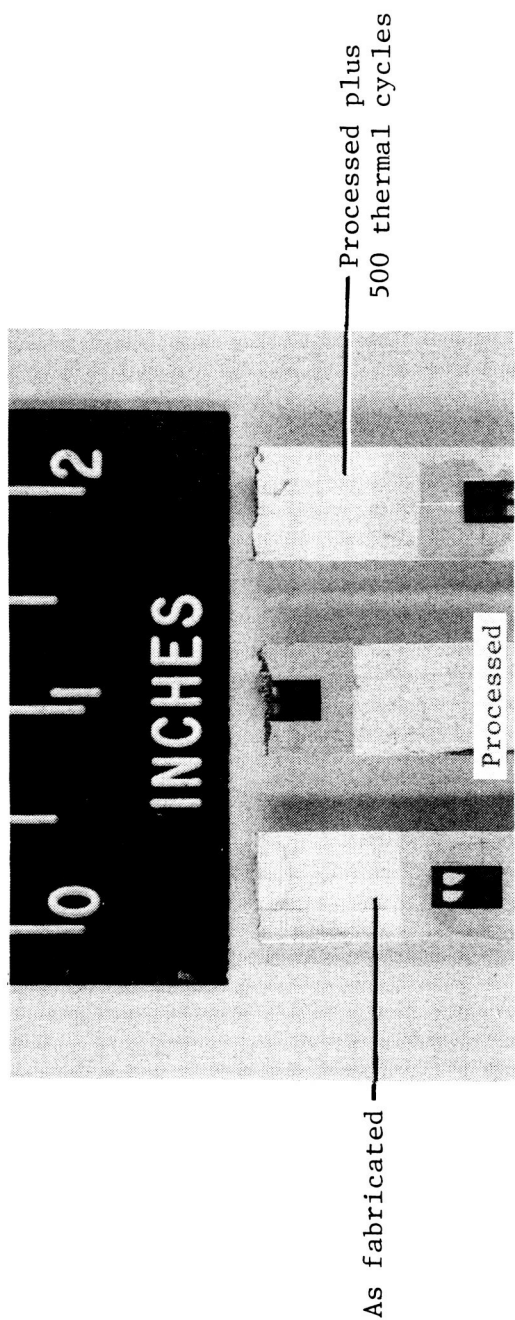
(a) Fracture profiles.
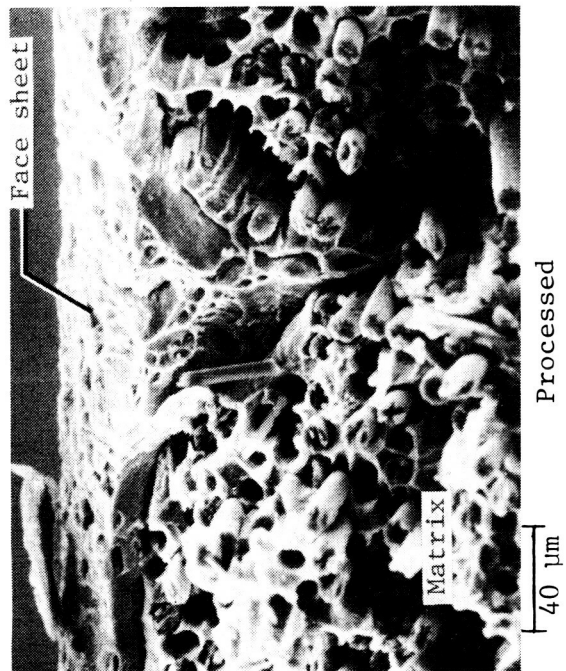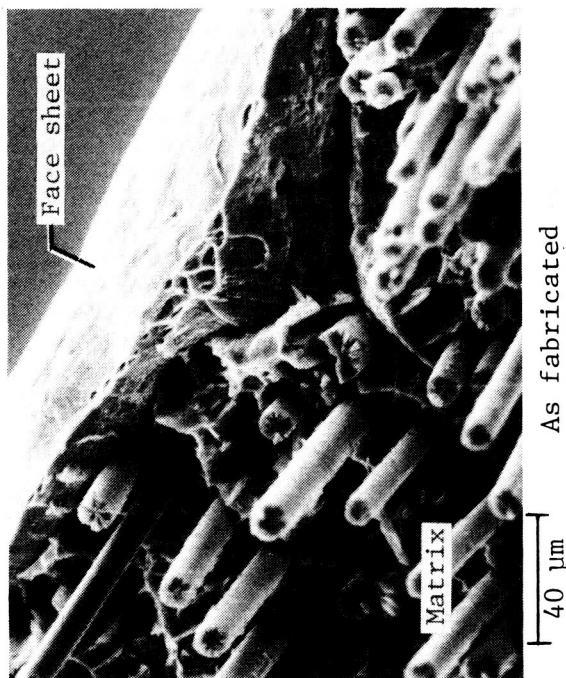
(b) Typical SEM fractographs.

Figure 13. Typical fracture profiles and SEM fractographs of diffusion-bonded P100 Gr/6061 Al composite specimens.

L-86-340
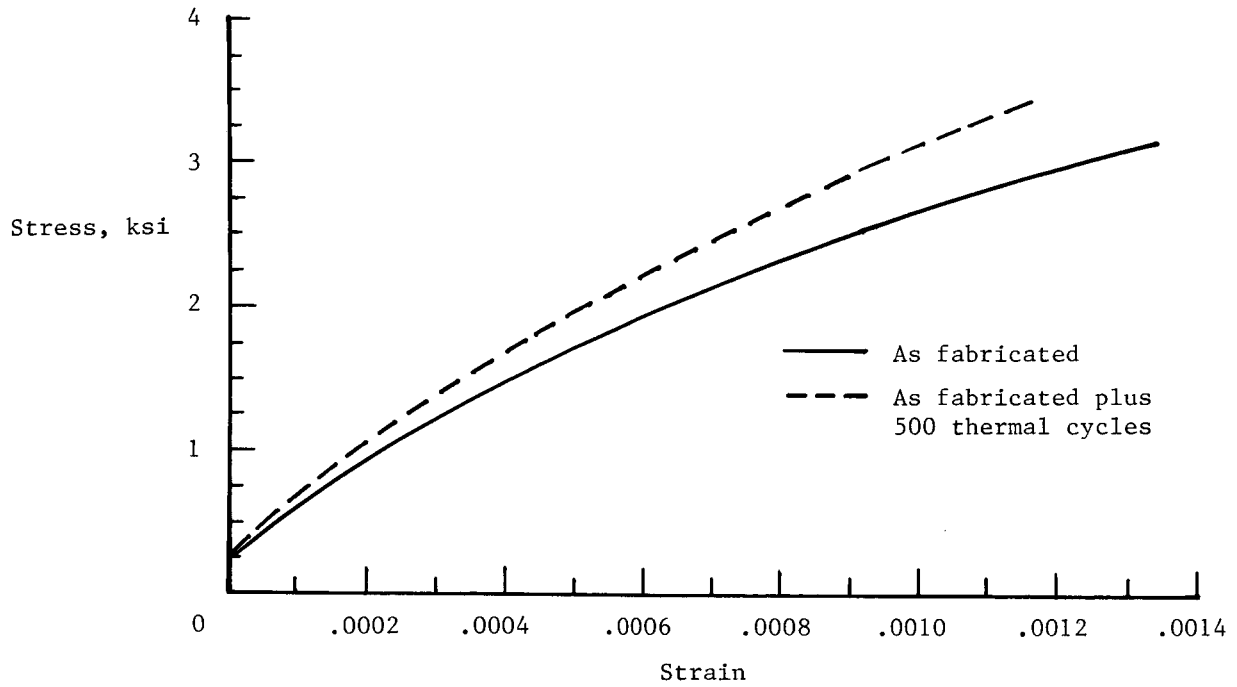
(a) As-fabricated specimen.
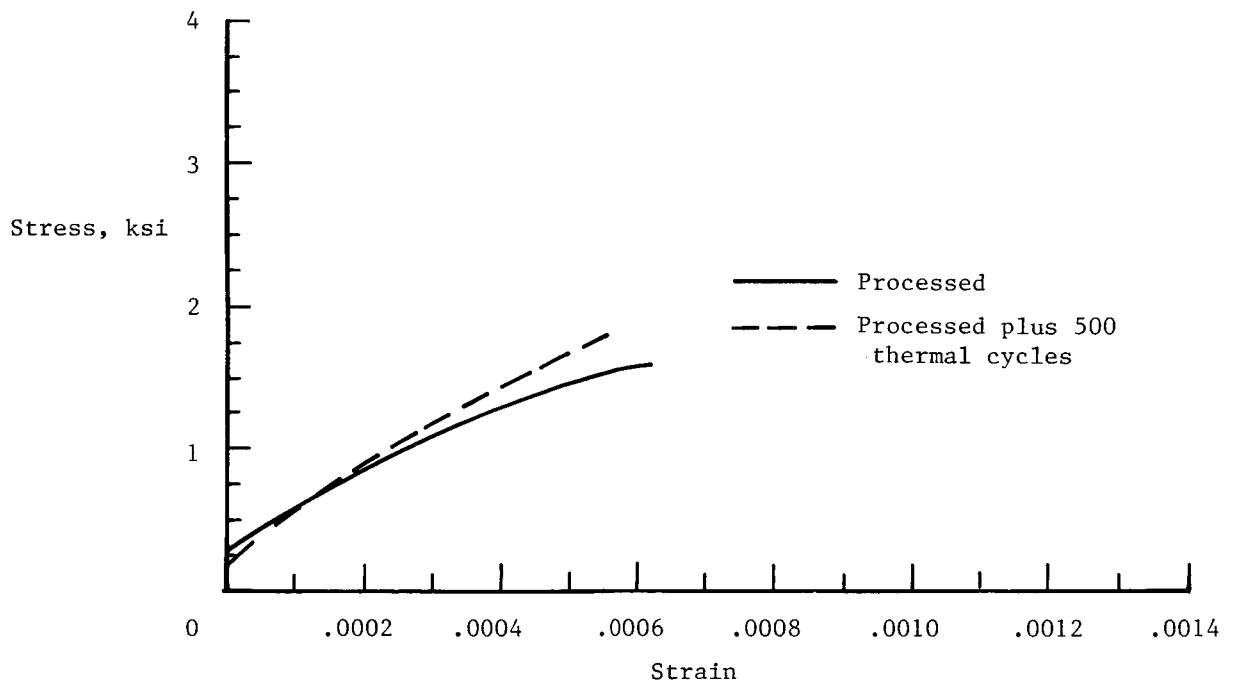
(b) Processed specimen.

Figure 14. Effect of thermal cycling on transverse tensile stress-strain behavior of diffusion-bonded P100 Gr/6060 Al composite.
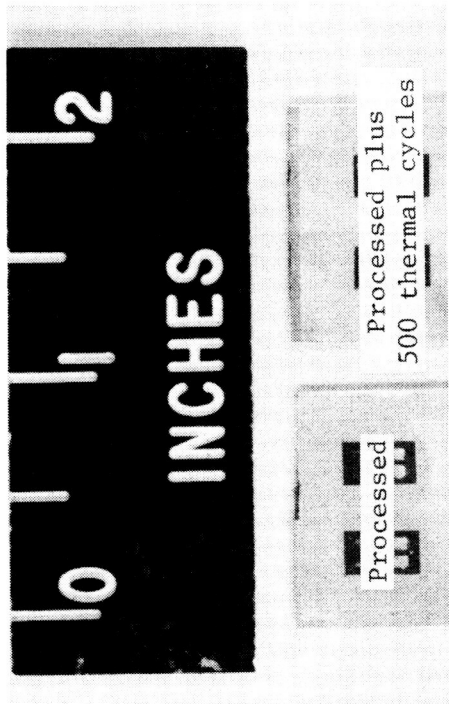
(a) Typical fracture profiles.
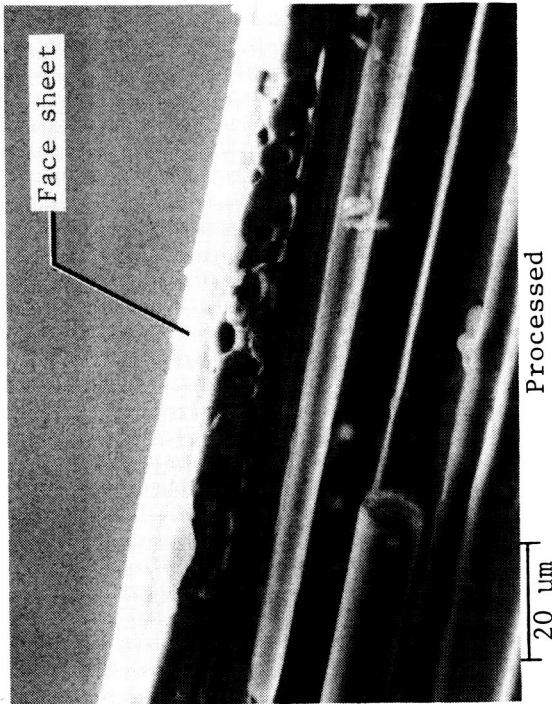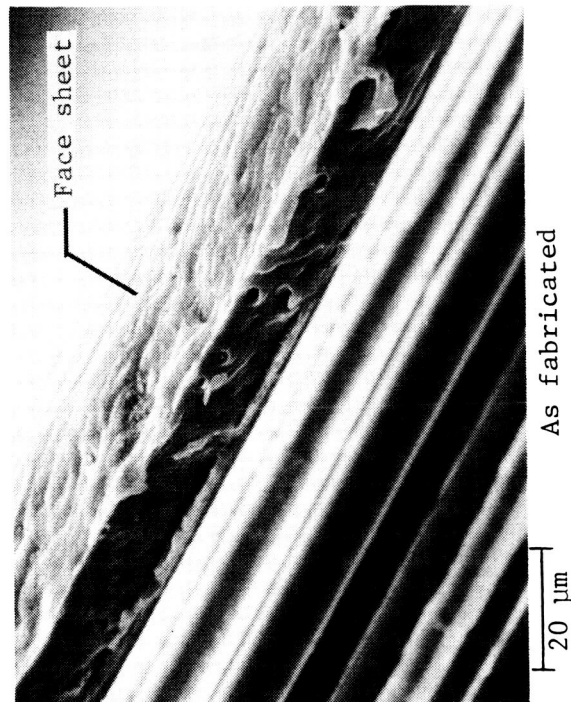
L-86-341

(b) Typical SEM fractographs.

Figure 15. Typical profiles and SEM fractographs of transversely loaded diffusion-bonded P100 Gr/6061 Al composite specimens.
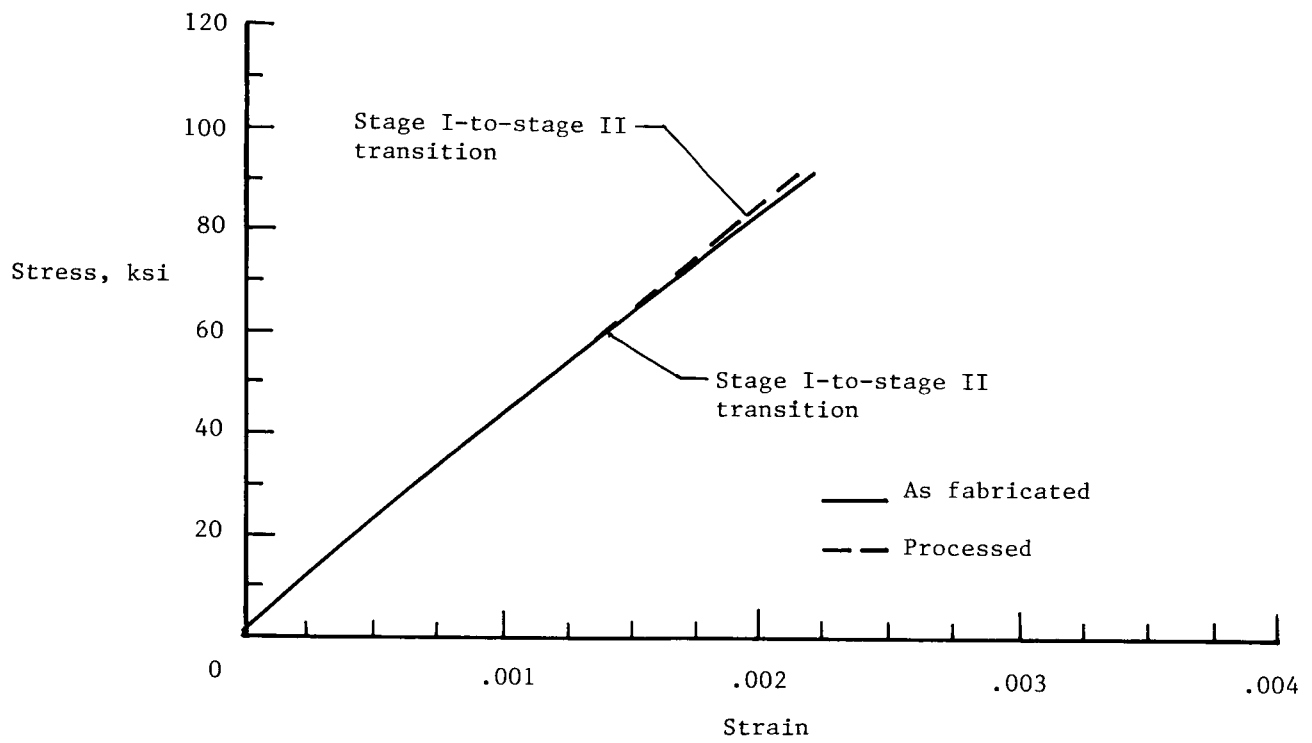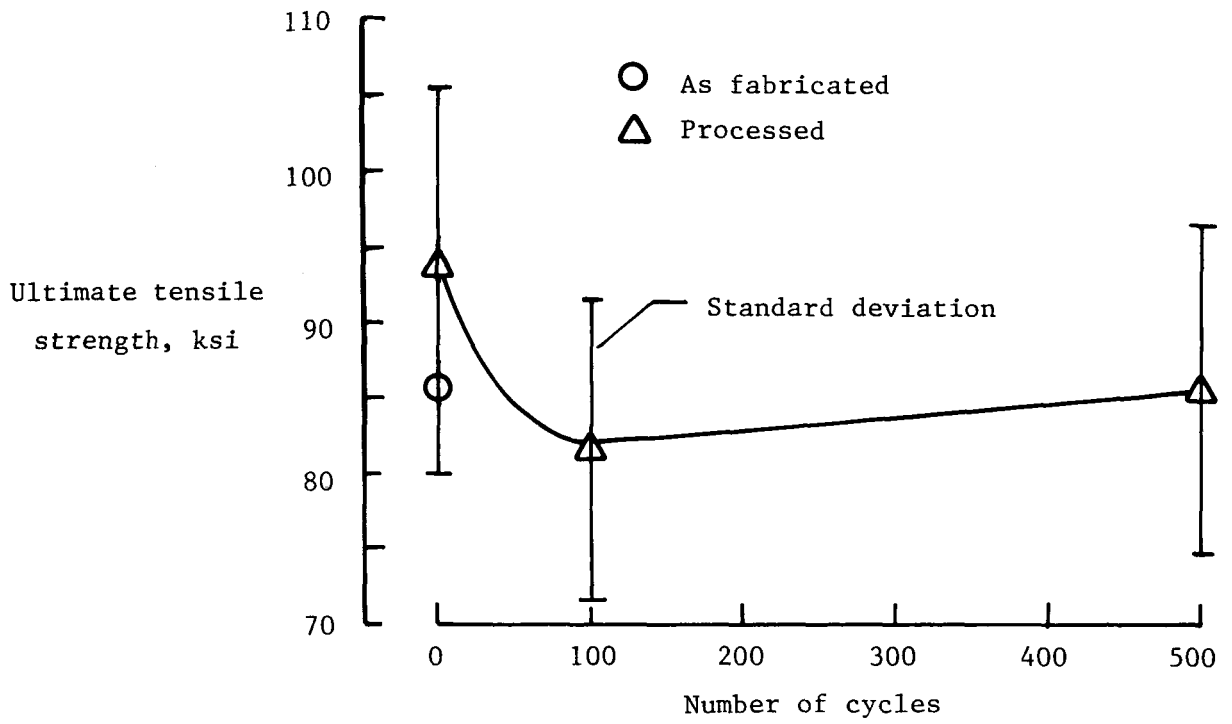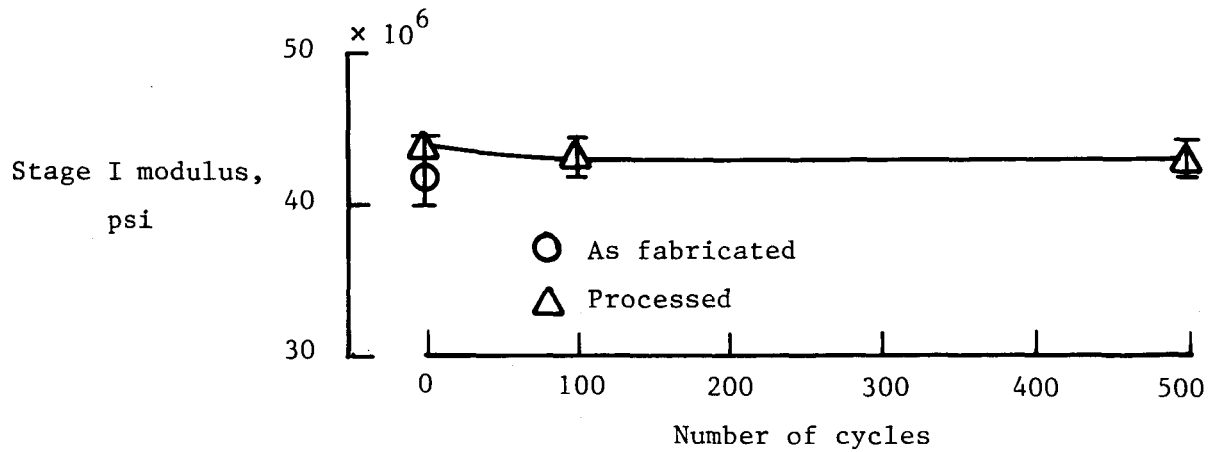
Figure 16. Typical longitudinal tensile stress-strain curves for hot-roll-bonded P100 Gr/6061 Al composites.
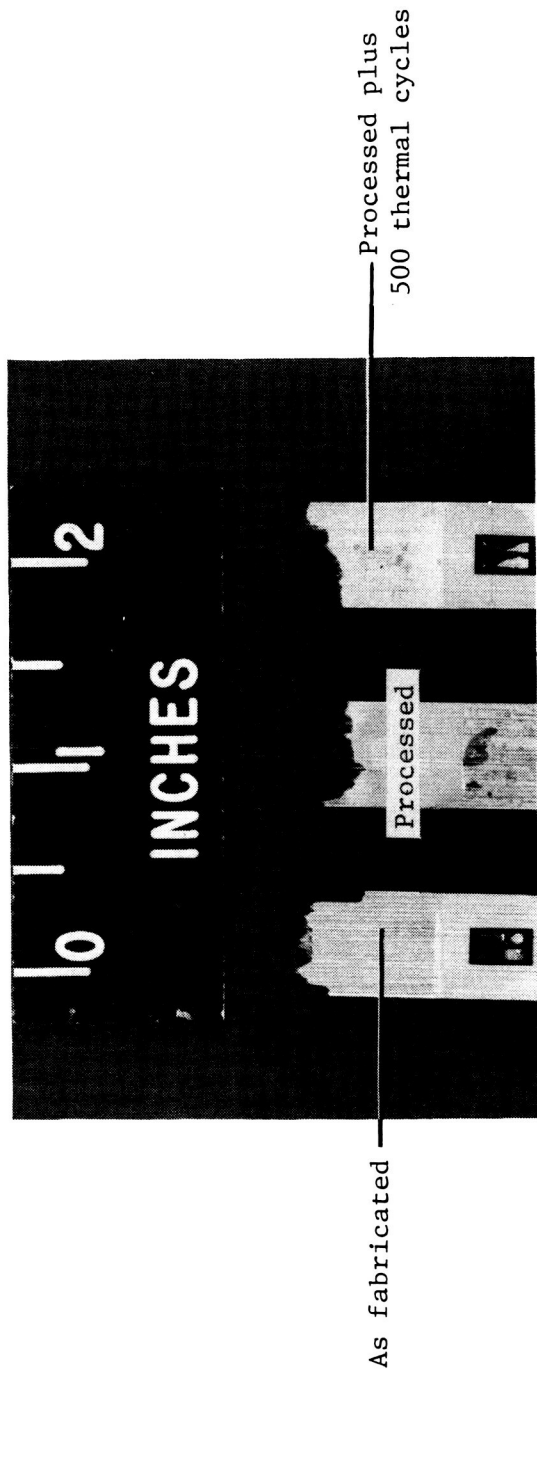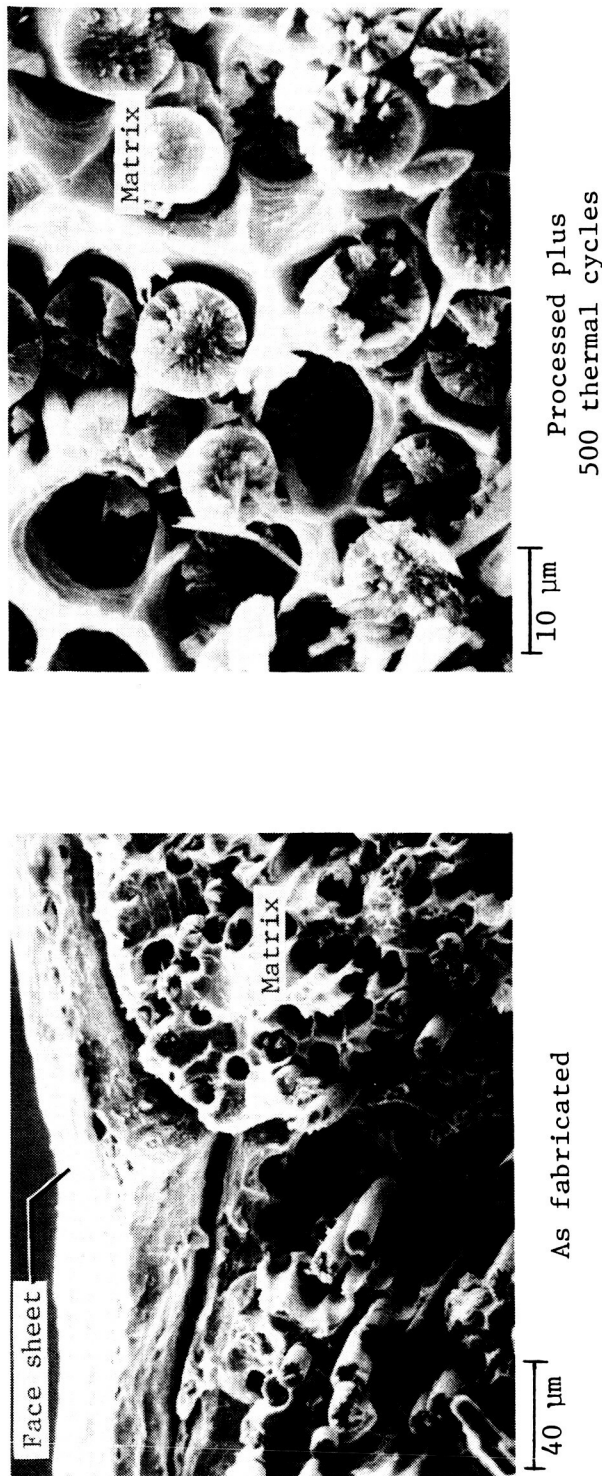
(a) Ultimate tensile strength.

(b) Stage I modulus.

Figure 17. Tensile properties for thermally cycled hot-roll-bonded P100 Gr/6061 Al composites.

(a) Fracture profiles.

(b) Typical SEM fractographs.

L-86-342

Figure 18. Typical fracture profiles and SEM fractographs of hot-roll-bonded P100 Gr/6061 Al composite specimens.

Standard Bibliographic Page

1. Report No. NASA TP-2612	2. Government Accession No.	3. Recipient's Catalog No.
4. Title and Subtitle Effects of Thermal Cycling on Graphite-Fiber-Reinforced 6061 Aluminum		5. Report Date October 1986
		6. Performing Organization Code 506-43-21-02
7. Author(s) Gregory A. Dries and Stephen S. Tompkins		8. Performing Organization Report No. L-16139
9. Performing Organization Name and Address NASA Langley Research Center Hampton, VA 23665-5225		10. Work Unit No.
		11. Contract or Grant No.
12. Sponsoring Agency Name and Address National Aeronautics and Space Administration Washington, DC 20546-0001		13. Type of Report and Period Covered Technical Paper
		14. Sponsoring Agency Code

15. Supplementary Notes

Gregory A. Dries: PRC Kentron, Inc., Hampton, Virginia.
Stephen S. Tompkins: Langley Research Center, Hampton, Virginia.

16. Abstract

Graphite-reinforced aluminum alloy metal-matrix composites are among materials being considered for structural components in dimensionally stable space structures. This application requires materials with low values of thermal expansions and high specific stiffnesses. They must remain stable during exposures to the space environment for periods extending to 20 years. The effects of thermal cycling on the thermal expansion behavior and mechanical properties of Thornel P100 graphite 6061 aluminum composites, as fabricated and after thermal processing to eliminate thermal strain hysteresis, have been investigated. Two groups of composites were studied: one was fabricated by hot roll bonding and the other by diffusion bonding. Processing significantly reduced strain hysteresis during thermal cycling in both groups and improved the ultimate tensile strength and modulus in the diffusion-bonded composites. Thermal cycling stabilized the as-fabricated composites by reducing the residual fabrication stress and increased the matrix strength by metallurgical aging. Thermal expansion behavior of both groups after processing was insensitive to thermal cycling. Data scatter was too large to determine effects of thermal cycling on the mechanical properties. The primary effects of processing and thermal cycling can be attributed to changes in the metallurgical condition and stress state of the matrix.

17. Key Words (Suggested by Authors(s)) Metal matrix Thermal expansion Thermal cycling Dimensional stability	18. Distribution Statement Unclassified—Unlimited Subject Category 24		
19. Security Classif.(of this report) Unclassified	20. Security Classif.(of this page) Unclassified	21. No. of Pages 29	22. Price A03